


















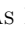




















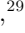




TOI-4562 b: A highly eccentric temperate Jupiter analog orbiting a young field star.

ALEXIS HEITZMANN ¹ GEORGE ZHOU ¹ SAMUEL N. QUINN ² CHELSEA X. HUANG ¹ JIAYIN DONG ^{3,4,5,*}
L. G. BOUMA ^{6,†} REBEKAH I. DAWSON ^{4,5} STEPHEN C. MARSDEN ¹ DUNCAN WRIGHT ¹ PASCAL PETIT ⁷
KAREN A. COLLINS ² KHALID BARKAOU ^{8,9,10} ROBERT A. WITTENMYER ¹ EDWARD GILLEN ^{11,12,‡}
RAFAEL BRAHM ^{13,14} MELISSA HOBSON ^{15,14} COEL HELLIER ¹⁶ CARL ZIEGLER ¹⁷ CÉSAR BRICEÑO ¹⁸
NICHOLAS LAW¹⁹ ANDREW W. MANN ¹⁹ STEVE B. HOWELL ²⁰ CRYSTAL L. GNILKA ²⁰ COLIN LITTLEFIELD ^{21,20}
DAVID W. LATHAM ² JACK J. LISSAUER ²² ELISABETH R. NEWTON ²³ DANIEL M. KROLIKOWSKI ²⁴
RONAN KERR ²⁴ RAYNA RAMPALLI ²³ STEPHANIE T. DOUGLAS ²⁵ NORA L. EISNER ²⁶ NATHALIE GUEDJ²⁷
GUOYOU SUN²⁷ MARTIN SMIT²⁷ MARC HUTEN²⁷ THORSTEN ESCHWEILER²⁷ LYU ABE²⁸ TRISTAN GUILLOT ²⁸
GEORGE RICKER ²⁹ ROLAND VANDERSPEK ²⁹ SARA SEAGER ^{30,29,31} JON M. JENKINS ²⁰ ERIC B. TING ²⁰
JOSHUA N. WINN ³² DAVID R. CIARDI ³³ ANDREW M. VANDERBURG ^{34,35} CHRISTOPHER J. BURKE ²⁹
DAVID R. RODRIGUEZ ³⁶ AND TANSU DAYLAN ^{32,37}

¹University of Southern Queensland, Centre for Astrophysics, West Street, Toowoomba, QLD 4350 Australia

²Center for Astrophysics | Harvard & Smithsonian, 60 Garden Street, Cambridge, MA 02138, USA

³Center for Computational Astrophysics, Flatiron Institute, 162 Fifth Avenue, New York, NY 10010, USA

⁴Department of Astronomy & Astrophysics, 525 Davey Laboratory, The Pennsylvania State University, University Park, PA, 16802, USA

⁵Center for Exoplanets and Habitable Worlds, 525 Davey Laboratory, The Pennsylvania State University, University Park, PA, 16802, USA

⁶Cahill Center for Astrophysics, California Institute of Technology, Pasadena, CA 91125, USA

⁷Institut de Recherche en Astrophysique et Planétologie, Université de Toulouse, CNRS, CNES, 14 avenue Edouard Belin, 31400 Toulouse, France

⁸Astrobiology Research Unit, Université de Liège, 19C Allée du 6 Août, 4000 Liège, Belgium

⁹Department of Earth, Atmospheric and Planetary Science, Massachusetts Institute of Technology, 77 Massachusetts Avenue, Cambridge, MA 02139, USA

¹⁰Instituto de Astrofísica de Canarias (IAC), Calle Vía Láctea s/n, 38200, La Laguna, Tenerife, Spain

¹¹Astronomy Unit, Queen Mary University of London, Mile End Road, London E1 4NS, UK

¹²Astrophysics Group, Cavendish Laboratory, J.J. Thomson Avenue, Cambridge CB3 0HE, UK

¹³Facultad de Ingeniería y Ciencias, Universidad Adolfo Ibáñez, Av. Diagonal las Torres 2640, Peñalolén, Santiago, Chile

¹⁴Millennium Institute of Astrophysics MAS, Nuncio Monsenor Sotero Sanz 100, Of. 104, Providencia, Santiago, Chile

¹⁵Max Planck Institute for Astronomy, Königstuhl 17, D-69117—Heidelberg, Germany

¹⁶Astrophysics Group, Keele University, Staffordshire, ST5 5BG, UK

¹⁷Department of Physics, Engineering and Astronomy, Stephen F. Austin State University, 1936 North St, Nacogdoches, TX 75962, USA

¹⁸Cerro Tololo Inter-American Observatory, Casilla 603, La Serena, Chile

¹⁹Department of Physics and Astronomy, The University of North Carolina at Chapel Hill, Chapel Hill, NC 27599-3255, USA

²⁰NASA Ames Research Center, Moffett Field, CA 94035, USA

²¹Bay Area Environmental Research Institute, Moffett Field, CA 94035, USA

²²Space Science & Astrobiology Division, MS 245-3, NASA Ames Research Center, Moffett Field, CA 94035, USA

²³Department of Physics and Astronomy, Dartmouth College, Hanover, NH 03755, USA

²⁴Department of Astronomy, The University of Texas at Austin, Austin, TX 78712, USA

²⁵Department of Physics, Lafayette College, 730 High St., Easton, PA 18042, USA

²⁶Sub-department of Astrophysics, University of Oxford, Keble Rd, Oxford, United Kingdom

²⁷Citizen Scientist, Zooniverse c/o University of Oxford, Keble Road, Oxford OX1 3RH, UK

²⁸Université Côte d'Azur, Observatoire de la Côte d'Azur, CNRS, Laboratoire Lagrange, CS 34229, F-06304 Nice Cedex 4, France

²⁹Department of Physics and Kavli Institute for Astrophysics and Space Research, Massachusetts Institute of Technology, Cambridge, MA 02139, USA

³⁰Department of Earth, Atmospheric, and Planetary Sciences, Massachusetts Institute of Technology, Cambridge, MA 02139, USA

³¹Department of Aeronautics and Astronautics, Massachusetts Institute of Technology, Cambridge, MA 02139, USA

³²Department of Astrophysical Sciences, Princeton University, Princeton, NJ 08544, USA

³³NASA Exoplanet Science Institute, Caltech/IPAC, 1200 E. California Ave, Pasadena, CA 91125, USA

³⁴Department of Physics and Kavli Institute for Astrophysics and Space Research, Massachusetts Institute of Technology, Cambridge, MA 02139, USA

³⁵Department of Astronomy, University of Wisconsin-Madison, Madison, WI 53706, USA

³⁶Space Telescope Science Institute, 3700 San Martin Drive, Baltimore, MD, 21218, USA

³⁷LSSTC Catalyst Fellow

ABSTRACT

We report the discovery of TOI-4562 b (TIC-349576261), a Jovian planet orbiting a young F7V-type star, younger than the Praesepe/Hyades clusters (< 700 Myr). This planet stands out because of its unusually long orbital period for transiting planets with known masses ($P_{\text{orb}} = 225.11781_{-0.00022}^{+0.00025}$ days), and because it has a substantial eccentricity ($e = 0.76_{-0.02}^{+0.02}$). The location of TOI-4562 near the southern continuous viewing zone of *TESS* allowed observations throughout 25 sectors, enabling an unambiguous period measurement from *TESS* alone. Alongside the four available *TESS* transits, we performed follow-up photometry using the South African Astronomical Observatory node of the Las Cumbres Observatory, and spectroscopy with the CHIRON spectrograph on the 1.5 m SMARTS telescope. We measure a radius of $1.118_{+0.013}^{-0.014} R_{\text{J}}$, and a mass of $2.30_{-0.47}^{+0.48} M_{\text{J}}$ for TOI-4562 b. The radius of the planet is consistent with contraction models describing the early evolution of the size of giant planets. We detect tentative transit timing variations at the ~ 20 min level from five transit events, favouring the presence of a companion that could explain the dynamical history of this system if confirmed by future follow-up observations. With its current orbital configuration, tidal timescales are too long for TOI-4562 b to become a hot-Jupiter via high eccentricity migration, though it is not excluded that interactions with the possible companion could modify TOI-4562 b's eccentricity and trigger circularization. The characterisation of more such young systems is essential to set constraints on models describing giant planet evolution.

1. INTRODUCTION

Planetary systems evolve rapidly within the first hundreds of millions of years of formation. The architectures of the systems evolve before settling into their eventual orbital configuration. Planets with extensive gaseous envelopes are expected to undergo contraction and cooling and experience observable changes in radius within this time frame. Observations of planets around young stars help anchor our understanding of this era of rapid change and help define models of planet formation and evolution. In particular, Jovian planets in distant orbits are less affected by stellar irradiation than close-in hot Jupiters. Transiting cold Jupiters around young stars can therefore provide constraints for cooling and contraction of giant planet evolution models. The orbital properties of these planets can also help to narrow down the timescales of dynamical evolution experienced by many other giant planets discovered to date.

Numerous mechanisms are responsible for the formation and evolution of close-in Jovian planets. These mechanisms vary by the distribution of planets that they

produce and by the timescales at which they operate. We can best assess the prevalence of these multiple formation channels via a census of the gas giant population as a function of time (see Dawson & Johnson 2018). Such a temporal survey of planetary systems can unveil the roles that in-situ formation (review in Chabrier et al. 2014), disk migration (review in Baruteau et al. 2014) and high eccentricity migration (review in Dawson & Johnson 2018) played in shaping our current gas giant population. For example, planets can gravitationally interact with their depleting gas disks, resulting in moderately eccentric final orbits within a few million years (e.g., Nagasawa et al. 2003; Duffell & Chiang 2015; Debras et al. 2021). On the other extreme, excitation via stellar fly-bys can occur on the hundreds of millions of years timescale (e.g., Shara et al. 2016).

Gas giants also undergo significant contraction in the first hundred million years post formation. In models, the rate of contraction is strongly dependent on the initial conditions of the planet post formation, such as their envelope-core mass ratio and initial luminosities (e.g., Fortney et al. 2007; Linder et al. 2019). It is clear, however, that the radius distribution of close-in Jovian planets is shaped by external factors that retard their contraction (e.g., Guillot & Showman 2002; Baraffe et al. 2003; Batygin & Stevenson 2010). Young planets

* Flatiron Research Fellow

† 51 Pegasi b Fellow

‡ Winton Fellow

in distant orbits provide simpler key tests for gas giant evolution.

Missions like Kepler, K2, and the Transiting Exoplanet Survey Satellite (*TESS*; Ricker et al. 2015) have brought forth a growing number of planetary systems about young stars (e.g., Newton et al. 2019; Mann et al. 2020; Plavchan et al. 2020; Bouma et al. 2022a,b; Zhou et al. 2022). However, true young Jovian analogues are rare. Interestingly, Suárez Mascareño et al. (2022) measured the masses of the giant planets in the 22 Myr old V1298 Tau system (David et al. 2019a,b), finding that the two Jovian planets have already settled to their expected final radii, a process that is predicted to take hundreds of millions of years by contraction models. Other close-in Jovian-sized planets have also been found around young stars (Rizzuto et al. 2020; Bouma et al. 2020; Mann et al. 2021), but strong stellar activity has yet prevented their mass from being measured.

We report the discovery of a young transiting Jovian planet in a distant orbit around a < 700 Myr old star. TOI-4562 hosts a temperate-Jupiter in a 225 day period orbit near the *TESS* continuous viewing zone. Along with additional observations from our ground-based photometric follow-up campaign, five total transits of the planet were obtained, unambiguously identifying the period of the system. Radial velocity monitoring over the following two years provided a mass and eccentricity measurement for the young planet. In addition, data from FEROS helped to constrain the stellar parameters, and high resolution images from Gemini-South and SOAR helped to rule out false positive scenarios, confirming the transit candidate as a true planet. We also constrained the age of TOI-4562 via gyrochronology and lithium. Finally we detect a transit timing variations (TTV) signature, indicative of a perturbing companion in the system. TOI-4562b is one of the longest period transiting temperate Jupiters discovered by *TESS*, and the youngest amongst such planets. Missions like *TESS* and *PLATO* (Rauer et al. 2014) have the potential to uncover this special population that critically constrains cooling models and migration pathways for Jovian planets.

2. OBSERVATIONS

2.1. *TESS: Photometry*

The transiting planet candidate around TOI-4562 was first identified from observations by *TESS*. TOI-4562 lies in the Southern Continuous Viewing Zone of *TESS*, and therefore received near-uninterrupted photometric monitoring during years 1 and 3 of operations. The target received observations at 30 minute cadence during Sectors 1-8 (2018-07-25 to 2019-02-28) and 10-13 (2019-

03-26 to 2019-07-18), and 2 minute target-pixel-stamp observations during sectors 27-39 (2020-07-04 to 2021-06-24). The transit signature of TOI-4562b was detected by the *TESS* Science Processing Operations Center (SPOC; Jenkins et al. (2016)) at NASA Ames Research Center during a transit search of sectors 27 through 39 with an adaptive, noise-compensating matched filter (Jenkins 2002; Jenkins et al. 2010, 2020). The transit signature passed all the diagnostic tests in the Data Validation report (Twicken et al. 2018) and was fitted with an initial limb-darkened transit model (Li et al. 2019). In particular, the transit signal passed the difference image centroiding test, which localized the source of the transits to within 1.0 ± 2.5 arcsec. The *TESS* Science Office reviewed the diagnostic information and released an alert to the community for TOI-4562b on 28 October 2021 (Guerrero et al. 2021).

We make use of the MIT Quicklook pipeline (Huang et al. 2020) photometric extraction from the Full Frame Image observations. In addition, where available, we make use of the 2 minute cadence target pixel file observations from the crowding and flux fraction corrected Simple Aperture Photometry (CROWDSAP) light curves (Twicken et al. 2010; Morris et al. 2020) made available by SPOC. Because of the large stellar variability seen in the light curve, we used the SAP light curves rather than the Pre-search Data Conditioning SAP (PDCSAP) flux and performed the detrending using a high order spline interpolation (Vanderburg & Johnson 2014)

The full *TESS* light curve covering all sectors of observations is presented in Figure 1. During the two (non-consecutive) years of near-continuous observations a total of 4 transits were captured by *TESS*. Figure 2 shows the zoomed in region around each of these transits.

TOI-4562 was first identified as a potential young star due to its strong rotational modulation (Zhou et al. 2021), as part of our program to survey for planets around young field stars. We performed a search for transiting signals around TOI-4562 via a Box-least-squares period search (Kovács et al. 2002) after removal of the stellar modulation signal with the splines. This detrending was not the one used for the transit modeling, described in section 4.1.

2.2. *Follow-up photometry*

We obtained follow-up photometric confirmation of the planetary transit via the Las Cumbres Observatory Global Network (LCOGT; Brown et al. 2013). Transit opportunities for a 225 day period planet are rare from the ground (see Table 3). We captured the full transit of TOI-4562 b on 2022-01-03 UTC from the South African

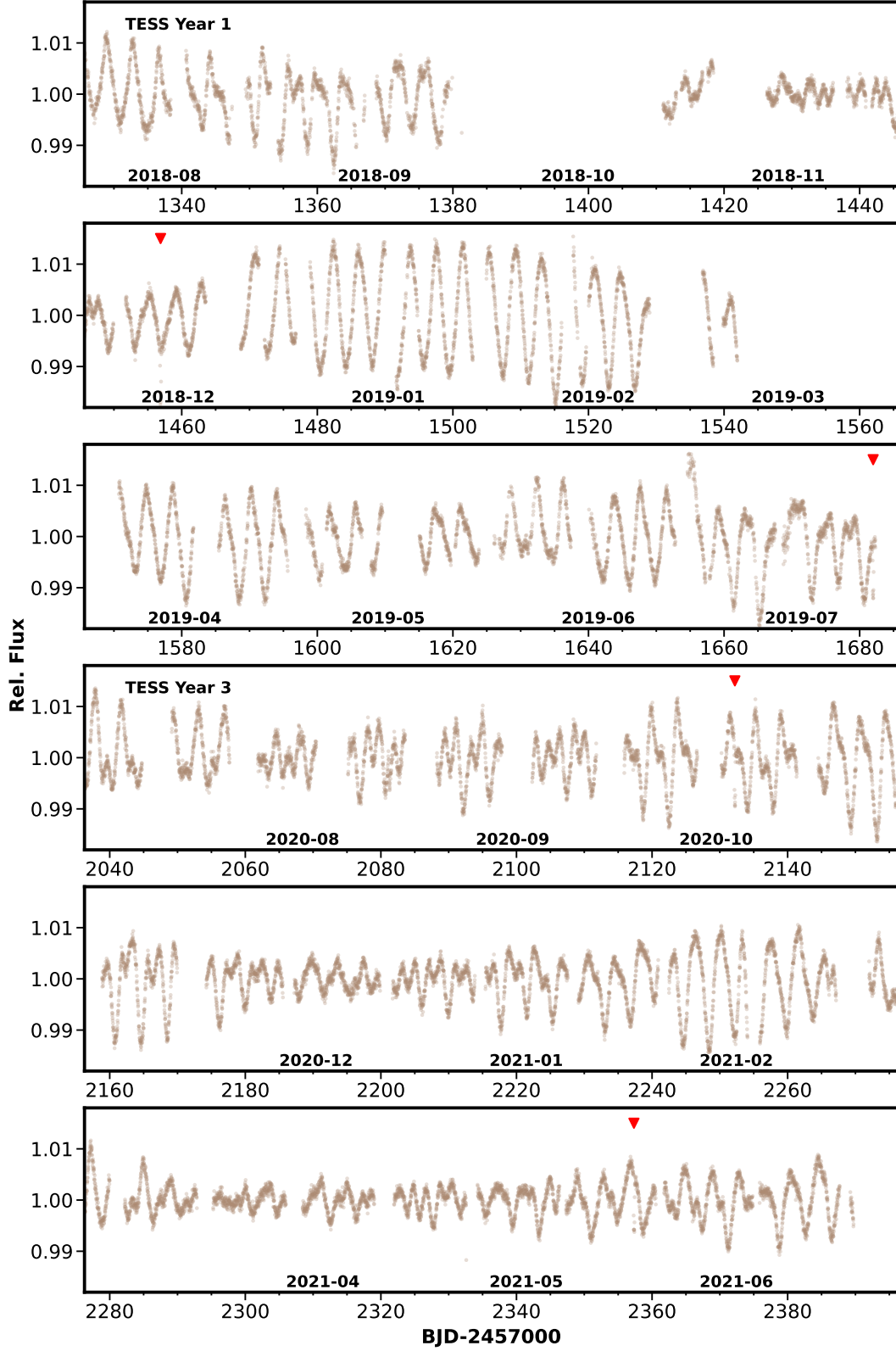


Figure 1. *TESS* lightcurve (brown) of TOI-4562 b from all 25 available sectors. Photometry prior to sector 13 were obtained at 30 minute cadence, while latter observations were obtained at 2 minute cadence, and binned in this figure to 30 min for clarity. The four TOI-4562 b transits from Sectors 5, 13, 30, and 38 are marked by red arrows. The host star exhibits up to $\sim 3\%$ peak-to-peak stellar rotational modulation due to its youth.

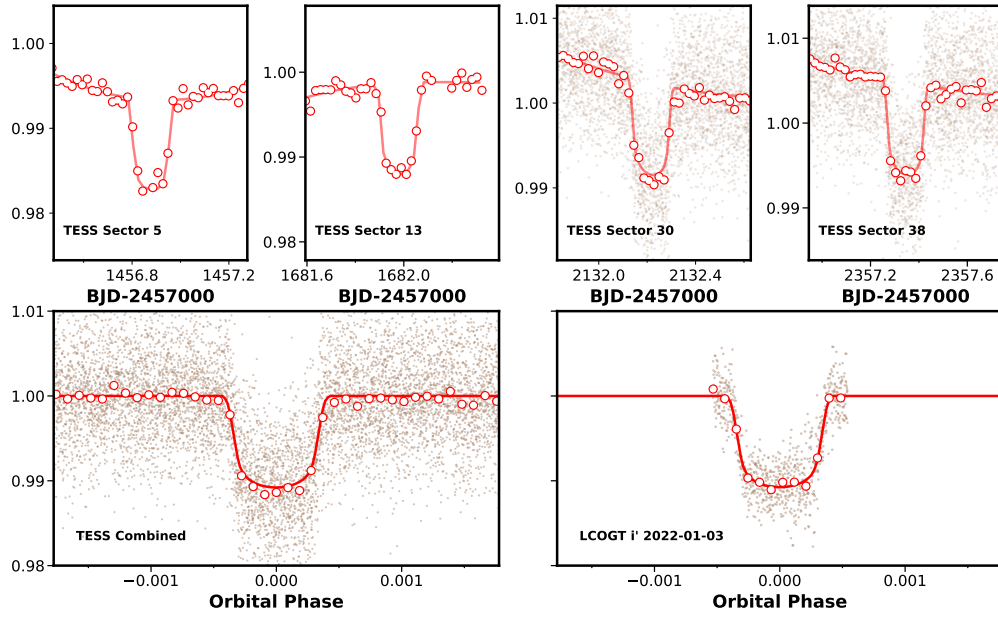


Figure 2. **Top** Individual transits from *TESS* from Sectors 5 and 13 at 30 minute cadence, and from Sectors 30 and 38 at 2 minute cadence. The red circles indicate the measured data for sectors 5 and 13, and the binned data at 30 minute cadence for Sectors 30 and 38. The 2-minute cadence data for Sectors 30 and 38 are plotted as brown points. The best fit model, incorporating the transit timing variations in Section 4, and out-of-transit trends, are shown by the red lines. **Bottom left** The phase folded *TESS* transit and best fit model. **Bottom right** The combined follow-up LCOGT 1 m observations from 2022-01-03 in i' band.

Astronomical Observatory (SAAO) node of LCOGT via two 1 m telescopes. The observations were obtained with the *Sinistro* 4K×4K cameras in the Sloan i' filter. The observations were calibrated via the BANZAI pipeline (McCully et al. 2018), and light curves were extracted via the ASTROIMAGEJ package (AIJ; Collins et al. 2017) using circular apertures with radius $4''.7$, which exclude flux from all known nearby Gaia EDR3 and TESS Input Catalog stars. The combined light curves (after removing systematics) and best fit model are shown in Figure 2.

In addition, a transit on 2022-08-16 was attempted from the SAAO node of LCOGT via one 1 m telescope, as well as the Antarctica Search for Transiting Exoplanets (ASTEP) facility (Guillot et al. 2015; Mékarnia et al. 2016), located at the East Antarctic plateau. A 25 minute segment was captured out of transit, but no portions of a transit event was recorded, and the dataset not included in the modeling presented below.

2.3. CHIRON/SMARTS: Spectroscopy

To characterize the radial velocity orbit of TOI-4562 b and constrain the properties of the host star, we obtained 84 spectroscopic observations of TOI-4562 using the CHIRON facility. To capture the long orbital period of TOI-4562 b, the velocities spanned two observing seasons, from 2020-12-09 to 2022-01-23; the resulting radial velocities are given in Table 4. CHIRON is a fiber-fed high resolution echelle spectrograph on the 1.5 m SMARTS telescope at Cerro Tololo Inter-American Observatory, Chile (Tokovinin et al. 2013). Due to the faintness of the host star, spectral observations were obtained in the ‘fiber’ mode of CHIRON, yielding a resolving power of $R \sim 28,000$ over the wavelength range of 4100 to 8700 Å, and an average signal-to-noise of ~ 100 per resolution element at the Mg b line wavelength region.

We make use of the extracted spectra from the standard CHIRON pipeline described in Paredes et al. (2021). Radial velocities were derived from the observations via a least-squares deconvolution against a non-rotating ATLAS9 spectral template (Castelli & Kurucz 2004). The resulting broadening profile is fitted via a kernel describing the effects of radial velocity shift, rotational, macroturbulent, and instrumental broadening. The derived velocities are presented in Table 4 and shown in Figure 4.

To estimate the spectroscopic properties of the host star, we matched each spectrum against an observed library of $\sim 10,000$ spectra pre-classified by the Spectroscopic Classification Pipeline (Buchhave et al. 2012). The matching was performed by first training the pre-

classified library via a gradient boosting classifier using SCIKIT-LEARN, and then classifying the observed spectrum. We found that TOI-4562 has an effective temperature of $T_{\text{eff}} = 6096 \pm 50$ K, a surface gravity of $\log g = 4.4 \pm 0.1$ dex, a bulk metallicity of $[M/H] = 0.1 \pm 0.1$ dex and a line of sight projected stellar rotational velocity of $v \sin i = 17 \pm 0.5$ km s $^{-1}$. Since the CHIRON dataset overwhelms the other datasets we obtained for TOI-4562 in quantity, we adopt these parameters as Gaussian priors in the global analysis of the system described in Section 4. We note a general consensus between the spectral parameters from CHIRON and those presented below in Section 2.4.

We also check for the possibility that the velocity variations we observe are due to a spectroscopically blended companion rather than the host star. We compare the broadening measured from the line profiles against the velocities and find no correlation. If a blended companion is causing the radial velocity offset, then the line profiles should be broadest at the orbital quadratures, and narrowest at conjunctions. We therefore find no evidence that the velocity variations originate from a blended companion.

2.4. FEROS & GALAH: Spectroscopy

The FEROS spectrograph, attached to the MPG 2.2 m (Kaufer et al. 1999) telescope at La Silla Observatory, gathered 11 spectra of TOI-4562. Spectra are co-added, with a signal to noise ratio per spectra ranging between 52 and 82, and atmospheric parameters are derived using ZASPE (Brahm et al. 2017b). We find $T_{\text{eff}} = 6280 \pm 100$ K, $\log g = 4.49 \pm 0.10$, $[M/H] = 0.24 \pm 0.05$ dex and $v \sin i = 15.7 \pm 0.5$ km s $^{-1}$. We chose not to include the FEROS data in the RV modelling. All points fall near phases (-0.4, 0.025 and 0.35) where the RV signal is close to 0 and therefore don’t meaningfully contribute, while adding one instrument and the associated extra parameters. Using the CERES pipeline (Brahm et al. 2017a), we also recover chromospheric emission indices, tracers of stellar activity. The core emission of the H $_{\alpha}$ line at 6562.808 Å is $H_{\alpha} = 0.160 \pm 0.005$ (following Boisse et al. (2009)). Using regions defined by Duncan et al. (1991) and calibrations from Noyes et al. (1984) we measure the core emission of the Ca II H and K lines around 3933 Å and 3968 Å to be $\log R'_{HK} = -4.503 \pm 0.044$. This value is consistent with a young active star (Mamajek & Hillenbrand 2008).

Finally, legacy spectra from the GALAH survey (Buder et al. 2021) found $T_{\text{eff}} = 6034 \pm 77$ K, $\log g = 4.36 \pm 0.18$, $[M/H] = 0.08 \pm 0.06$ and $v \sin i = 15.6 \pm 2.2$ km s $^{-1}$.

2.5. Gemini-South and SOAR: High resolution direct Imaging

A first high resolution image of TOI-4562 was obtained on 2022-03-17 with the Zorro Speckle camera on the 8.1 m Gemini-South telescope (Howell & Furlan 2022) and is shown in the top of Figure 3. Simultaneous observations were obtained at 562 and 832 nm respectively. Contrast curves were retrieved following Howell et al. (2011) for both wavelengths and neither shows sign of a companion in the vicinity of TOI-4562 b. A difference in magnitude Δm of 5 is achieved at a separation of $\sim 0.1''$. This allows us to rule out the presence of bright stellar objects in the same TESS pixel as TOI-4562 that would meaningfully impact the transit light curve to a projected distance of ~ 35 au (given TOI-4562’s distance of 350.0 ± 1.2 pc).

On 2022-04-19, another high resolution image was acquired with the HRCam instrument on the 4.1 m Southern Astrophysical Research (SOAR) telescope. TOI-4562 was observed as part of the SOAR TESS survey (Ziegler et al. 2020, 2021), and the data was reduced following Tokovinin (2018). The image shown in the bottom panel of Figure 3 and shows a contrast in the *I*-band of 5 mag within $1''$ with no sign of a companion, in agreement with the Gemini-South observation.

3. AGE OF TOI-4562

TOI-4562 does not appear in the extensive list of stars with known age and/or belonging to associations and moving groups compiled from the literature in Bouma et al. (2022). Similarly, we do not identify a co-eval population when applying the COMOVE package (Tofflemire et al. 2021) that uses Gaia DR3 astrometric parameters to find whether a given possible young star candidate is co-moving with its visual neighbours.

This lack of evidence of TOI-4562 belonging to any known moving group or open cluster means its age estimation is challenging. The variability seen in both photometry and radial velocity are indicative of the presence of rotationally modulated surface brightness features, likely due to the presence of dark spots and bright plages/faculae. Combined with a fast rotation period ($P_{\star} = 3.86_{-0.08}^{+0.05}$ days), this strongly suggests that TOI-4562 is a young and active star.

Determining the age of a field star is notoriously difficult (Soderblom 2010). In the following paragraphs, we make use of the rotation and lithium abundance of TOI-4562 to qualitatively assess its youth. We note that though TOI-4562 exhibits signatures of activity and youth indicative of being younger than 1 Gyr, pinpointing its age will remain difficult without placing it within co-moving populations. With increasingly more

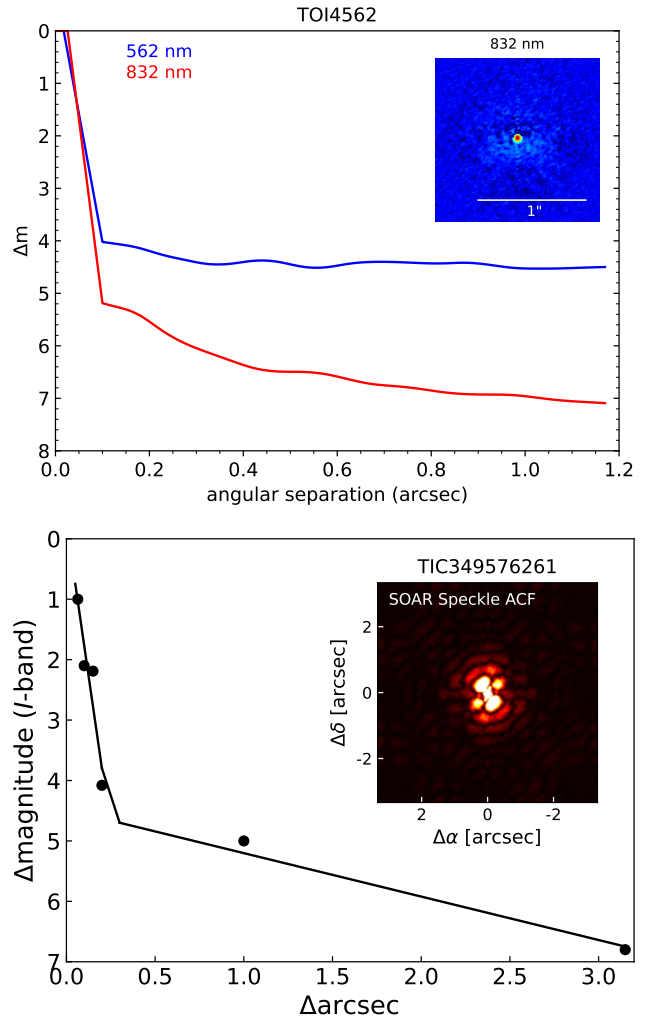


Figure 3. **Top** High resolution image of TOI-4562 obtained with the Zorro camera attached to the 8.1 m Gemini South telescope. The blue and red curves show difference in magnitude as a function of orbital separation from TOI-4562 obtained at wavelengths of respectively 562 and 832 nm. The inset plot shows the reconstructed image at 832 nm where no companion is detected. **Bottom** SOAR HRCam high resolution imaging of TOI-4562. The difference in magnitude as a function of orbital separation from TOI-4562 is shown by the black line and the autocorrelation function on the inset image. There is no sign of a stellar sized companion to TOI-4562.

sophisticated clustering with updated *Gaia* datasets, we hope that kinematics studies such as Oh et al. (2017), Gagné et al. (2018), Kounkel & Covey (2019) and Ujjwal et al. (2020) can provide improved census of young associations and groups.

3.1. Stellar rotation and Gyrochronology

Table 1. TOI-4562 parameters.

Parameters	Description	Prior	Value	Reference
Name and position				
TOI	<i>TESS</i> Object of Interest	-	4562	
TIC	<i>TESS</i> Input Catalog	-	349576261	ST18
<i>Gaia</i>	DR2 Source ID	-	5288681857665822080	<i>Gaia</i> EDR3
RA	Right ascension (HH:MM:SS, J2000, epoch 2015.5)	-	07:28:02.41	<i>Gaia</i> EDR3
DEC	Declination (DD:MM:SS, J2000, epoch 2015.5)	-	-63:31:04	<i>Gaia</i> EDR3
μ_{RA}	RA proper motion (mas yr ⁻¹)	-	-5.899 ± 0.015	<i>Gaia</i> EDR3
μ_{DEC}	DEC proper motion (mas yr ⁻¹)	-	10.491 ± 0.011	<i>Gaia</i> EDR3
Type	Spectral type	-	F7V	
ϖ	Parallax (mas)	$\mathcal{G}[2.857, 0.05]^a$	2.85692 ^{+0.01009} _{-0.00990}	This work
D	Distance (parsec)	-	350.0 ± 1.2	This work
Photospheric parameters				
T_{eff}	Effective temperature (K)	-	6096 ± 32 K	This work (CHIRON)
log g	Surface gravity (dex)	-	4.39 ± 0.01	This work
[M/H]	Bulk metallicity (dex)	$\mathcal{G}[0.2, 0.3]$	0.08 ± 0.06	This work
$v \sin i$	Rotational velocity (km s ⁻¹)	-	17 ± 0.5	This work (CHIRON)
Physical parameters				
M_{\star}	Mass (M_{\odot})	$\mathcal{U}[0, 2]$	1.192 ± 0.057	This work
R_{\star}	Radius (R_{\odot})		1.152 ± 0.046	This work
Age	Age (Myr)		< 700	This work
Activity parameters				
P_{\star}	Equatorial rotation period (days)	-	3.86 ^{+0.05} _{-0.08}	This work
Li 6708 EW	Li doublet ($\sim 6708 \text{ \AA}$) equivalent width (\AA)	-	0.076 ± 0.022	This work
log R'_{HK}		-	-4.503 ^{+0.028} _{-0.052}	This work (FEROS)
Photometric parameters				
E(B-V)	Interstellar extinction (mag)	$\mathcal{U}[0, 0.1542]^b$	< 0.01 (3 σ)	This work
T	<i>TESS</i> T (mag)	-	11.533 ± 0.006	ST18
V	Johnson V (mag)	-	12.098 ± 0.014	H16
B	Johnson B (mag)	-	12.698 ± 0.025	H16
G	<i>Gaia</i> G (mag)	-	11.948 ± 0.020 ^c	<i>Gaia</i> EDR3
B_p	<i>Gaia</i> B_p (mag)	-	12.262 ± 0.020 ^c	<i>Gaia</i> EDR3
R_p	<i>Gaia</i> R_p (mag)	-	11.467 ± 0.020 ^c	<i>Gaia</i> EDR3
J	2MASS J (mag)	-	10.931 ± 0.023	SK06
H	2MASS H (mag)	-	10.693 ± 0.025	SK06
K_s	2MASS K_s (mag)	-	10.619 ± 0.023	SK06
W_1	WISE W_1 (mag)	-	10.578 ± 0.023	W10,C13
W_2	WISE W_2 (mag)	-	10.618 ± 0.020	W10,C13
W_3	WISE W_3 (mag)	-	10.590 ± 0.061	W10,C13
NUV	GALEX/NUV calibrated AB magnitude (mag)	-	17.133 ± 0.023	B17

^aAdopted from *Gaia* EDR3 [Gaia Collaboration et al. \(2016, 2021\)](#), corrected using a zero point offset value of -0.024 mas, following [Lindegren et al. \(2021a\)](#)

^bAdopted from [Schlafly & Finkbeiner \(2011\)](#)

^cThese are inflated uncertainties from the *Gaia* photometric bands, following the convention from [Eastman et al. \(2013\)](#)

Priors: $\mathcal{U}[a, b]$ uniform priors with boundaries a and b ; $\mathcal{G}[\mu, \sigma]$ Gaussian priors

References: *Gaia* EDR3 [Gaia Collaboration et al. \(2016, 2021\)](#); ST18 [Stassun et al. \(2018\)](#); SK06 [Skrutskie et al. \(2006\)](#); W10 [Wright et al. \(2010\)](#); C13 [Cutri et al. \(2021\)](#); B17 [Bianchi et al. \(2017\)](#); H16 [Henden et al. \(2016\)](#)

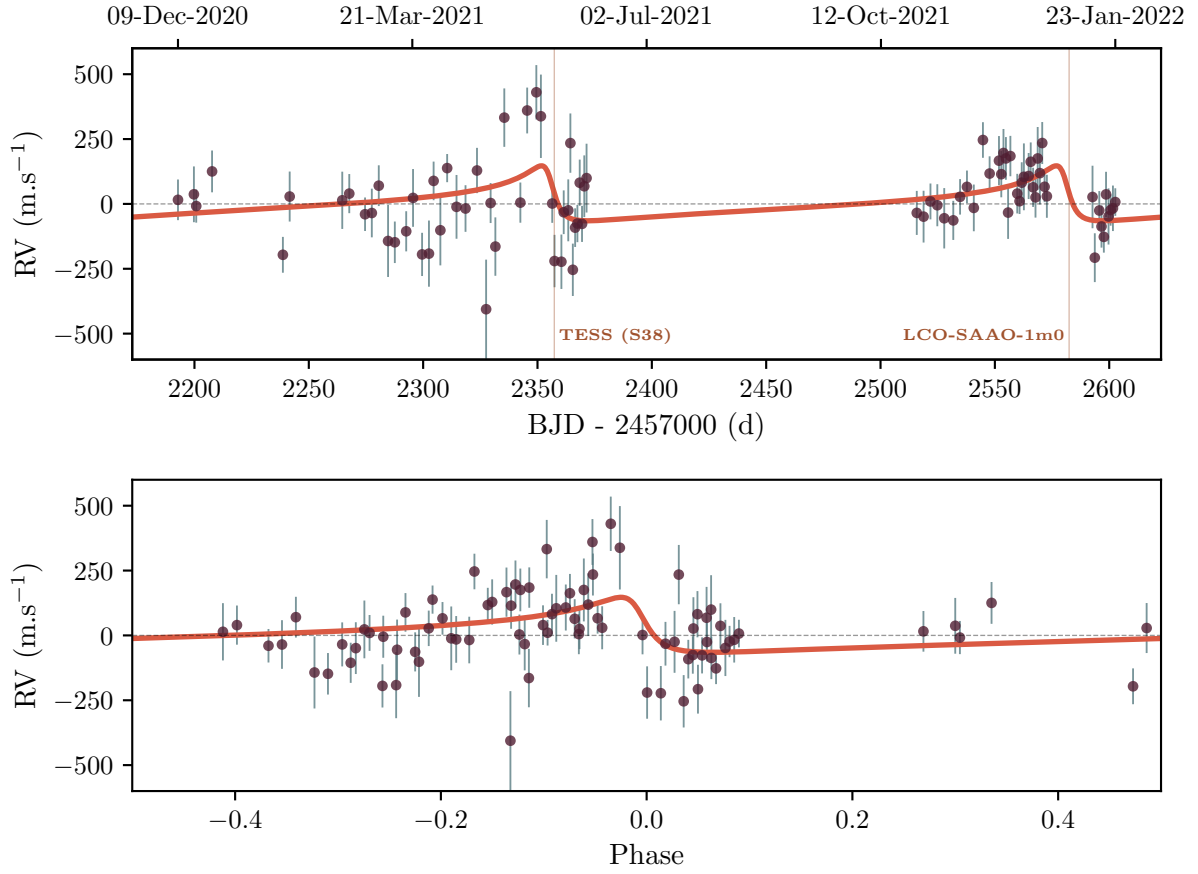


Figure 4. Top: 2-year radial velocity time series of TOI-4562 obtained with the CHIRON spectrograph (brown points) with the associated error bars. The Keplerian orbit fit from our global modelling is shown in red. Transits are highlighted in light brown. **Bottom:** Phase folded RVs (brown) with the Keplerian orbit best fits in red.

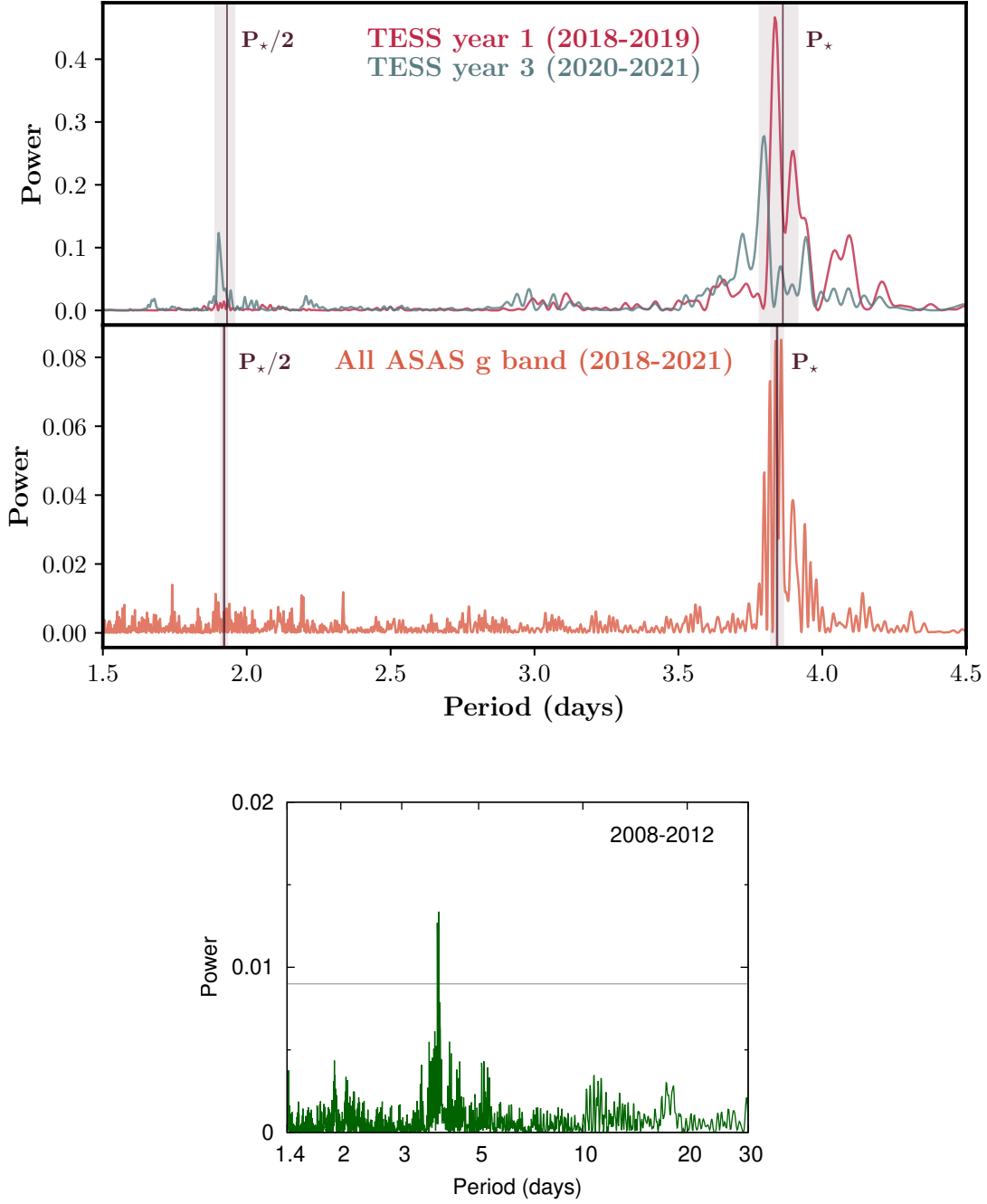


Figure 5. **Top** GLS periodogram of TOI-4562’s photometry from *TESS* for the first (2018-2019, red line) and third (2020-2021, blue line) year of data. The identified stellar rotation period ($P_* = 3.86^{+0.05}_{-0.08}$) and the first harmonic ($P_*/2$) are shown with the vertical brown lines with the surrounding shaded areas representing uncertainties. **Middle** GLS periodogram of ASAS-SN’s photometry gathered between 2018 and 2021 (orange line). The identified stellar rotation period ($P_* = 3.84 \pm 0.02$) and the first harmonic ($P_*/2$) are shown as the vertical brown lines with their respective uncertainties (shaded area). **Bottom** Periodogram on the 4 years (2008-2012) of WASP data yielding P_* estimates between 3.74 and 3.84 depending on the considered year. In all three periodograms, we notice a strong peak multiplicity around 3.9 days that could be associated with stellar surface features tracing differential rotation.

Young stars on the zero-age main-sequence spin rapidly. Over the course of a few billion years, mass loss from stellar winds spin-down Sun-like stars. The rotation period of Sun-like stars can be a tracer for their age. Rotation–colour–age relationships such as those from Barnes (2007) and Mamajek & Hillenbrand (2008) are calibrated against co-eval clusters and associations, and can provide useful metrics to estimate stellar ages. Recent theoretically-motivated models, which are based in wind braking models and can incorporate core-envelope coupling, also provide such relationships (e.g. Spada & Lanzafame 2020).

The 25 sectors of observations gathered by *TESS* provide the means for a good estimation of the rotation period of TOI-4562. As shown in Figure 5, we ran the PYASTRONOMY implementation of the Generalized Lomb-Scargle periodogram (GLS, Lomb 1976; Scargle 1982; Zechmeister & Kürster 2009) on the entire dataset and measured a rotation period of $P_{\star} = 3.86^{+0.05}_{-0.08}$ days. To obtain P_{\star} , we first computed separate GLS periodograms for individual sectors (each covering $\sim 7 P_{\star}$) previously binned to 10 minute cadence. The median and $1-\sigma$ values of all obtained periods were then used to derive P_{\star} and the associated uncertainties.

We note the clear second periodogram peak on Figure 5, close to P_{\star} . This could be showing differential rotation (i.e., the variation of P_{\star} as a function of stellar latitude). This has been largely observed in Kepler stars (Reinhold et al. 2013). We could suppose that the rotational modulation of two distinct clumps of surface stellar spots evolving at a different latitude would be at origin of the double peak (Lanza et al. 1993).

In addition, TOI-4562 received 4 years of monitoring with the Wide Angle Search for Planets (WASP) Consortium (Pollacco et al. 2006) Southern SuperWASP facility from 2008-2012. WASP-South is located at SAAO, and consists of an array of eight commonly mounted 200 mm f/1.8 Canon telephoto lenses, each with a 2K×2K detector. A period analysis of the WASP-South light curves reveals periods of 3.74, 3.84, 3.82 and 3.84 days for the 2008/2009, 2009/2010, 2010/2011 and 2011/2012 respectively, in agreement with the *TESS* light curves. The long term stability of the signal helps to confirm it as the correct alias of the rotational modulation signal. We note that WASP did not cover any transit event.

Finally, we run periodograms on the available light curves from the All-Sky Automated Survey for Supernovae (ASAS-SN, Shappee et al. (2014); Jayasinghe et al. (2019)). Sloan g-band data spanning from October 2017 to April 2022 shows very strong peaks in the periodogram at 3.84, 3.87 and 3.82 days for the

2018/2019, 2019/2020 and 2020/2021 seasons respectively (2017 and 2022 datasets are of poorer quality), agreeing with the other photometric datasets. Johnson V-band data was obtained between October 2016 and September 2018. Despite being less extensive and less densely sampled than the g-band photometry, a moderate peak (FAP $\sim 0.2\%$) is found at 3.64 days, close to P_{\star} .

Using the age-rotation relationship from Mamajek & Hillenbrand (2008), we found TOI-4562 b to be 110-490 (3σ) Myr old. We note that age estimates from this relationship assumes that the star lies on the slow-sequence of the age-rotation relationship. Stars are often found to be more rapidly rotating than such sequences for a given age, which has been attributed to binarity in cluster populations (e.g., Douglas et al. 2016; Gillen et al. 2020). Though there is no evidence for TOI-4562 being part of a binary system, caveats still apply for gyrochronology-based age estimates. For a $1.2 M_{\odot}$ star with $P_{\star} = 3.86^{+0.05}_{-0.08}$, the model from Spada & Lanzafame (2020) gives a consistent age estimate of 300-400 Myr.

The top plot of Figure 6 shows the rotation period of TOI-4562 compared with stars of known nearby clusters and associations. TOI-4562’s P_{\star} is consistent with that of stars belonging to Group X (Newton et al. 2022; Messina et al. 2022), with an estimated age of 300 Myr.

3.2. Lithium

The convective envelope of low-mass stars ($M_{\star} < 1.5 M_{\odot}$) allows efficient transport of lithium to deeper and hotter regions in a star’s interior, where it gets destroyed by proton capture. Calibrated with stars in clusters and associations, this lithium depletion can be used as a proxy for stellar age. Using CHIRON spectra (see section 2.3), we measured the equivalent width of the lithium doublet at 6707.76 and 6707.91 Å. We fit two Gaussian line profiles of the same depth at the respective wavelengths of the lithium doublet and one auxiliary with a different depth to account for the nearby Fe I line at 6707.43 Å, usually blended with the Li doublet. All profiles share the same width as per the rotational broadening of the star. We measure a lithium equivalent width of 0.084 ± 0.007 Å from a median combined spectrum of all our CHIRON observations. These data are displayed in Figure 6. On the same figure, we show the lithium equivalent width as function of effective temperature for stars belonging to clusters with well constrained ages, the Pleiades (~ 125 Myr), Group X (~ 300 Myr) and Praesepe (~ 670 Myr). TOI-4562 exhibits a Li equivalent width shallower than most of the Pleiades stars and of comparable strength to stars from the Praesepe cluster, at an effective temperature

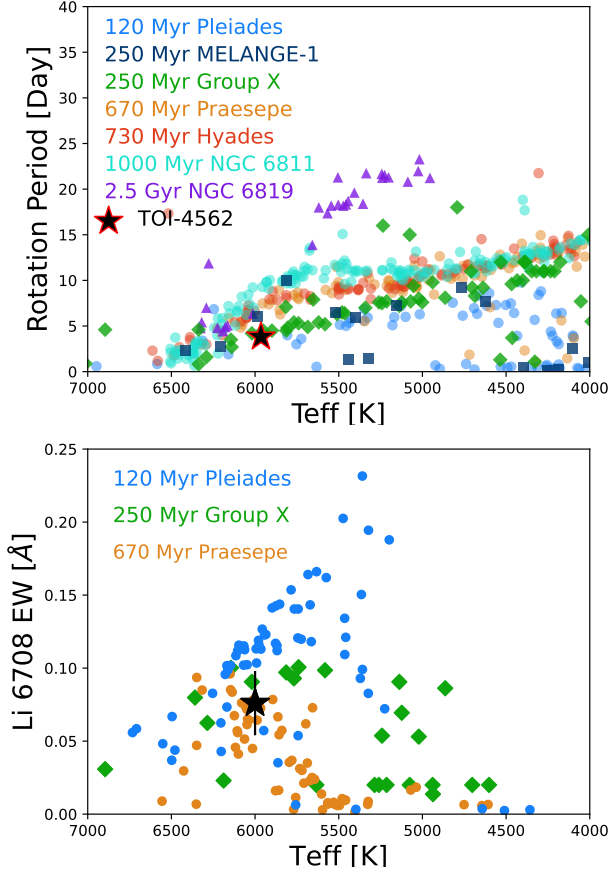


Figure 6. Youth indicators for TOI-4562. **Top:** The rotation period of TOI-4562 compared to the distribution of stars within known associations and clusters, including the Pleiades (Rebull et al. 2016), MELANGE-1 (Tofflemire et al. 2021), Group X (Newton et al. 2022; Messina et al. 2022), Praesepe and Hyades (Douglas et al. 2016, 2019), NGC 6811 (Curtis et al. 2019) and NGC 6819 (Meibom et al. 2015). **Bottom:** Equivalent width of the lithium doublet at 6707.76 and 6707.91 Å for TOI-4562 (red star) and stars in the Praesepe (orange, Cummings et al. 2017), Group X (Newton et al. 2022), and Pleiades (black, Bouvier et al. 2018) clusters. TOI-4562 lies at an age comparable to the Hyades and Praesepe.

of 6000 K. Combined with the Gyrochronology analysis, TOI-4562’s age is consistent with a star younger than the Praesepe/Hyades clusters (i.e., $\lesssim 700$ Myr).

3.3. Lithium, $\log R'_{HK}$ and $B - V$

Finally, we used the more recent BAFFLES package (Stanford-Moore et al. 2020) to derive an age estimate. BAFFLES is a Bayesian framework in which lithium abundance, the $\log R'_{HK}$ index and $B - V$ colour are used to infer an age posterior for the studied star. The likelihood functions used are calibrated against star belonging to open clusters and associations (i.e., with well constrained ages). For $\log R'_{HK} = -4.503$ (from

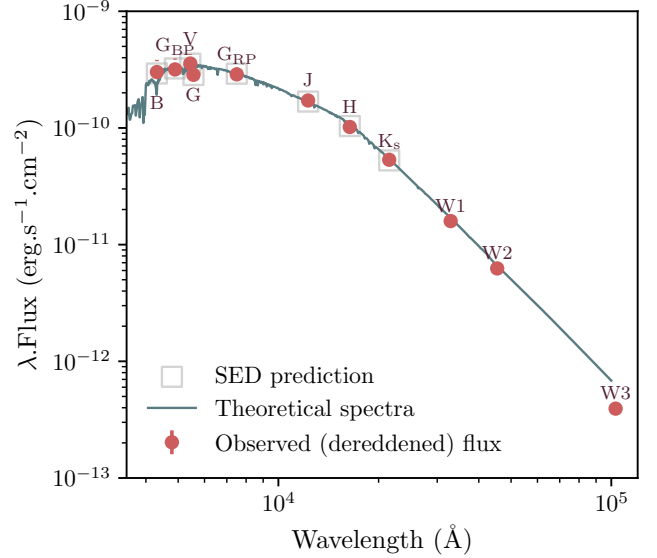


Figure 7. Spectral energy distribution (SED) of TOI-4562 b. Red points are the observed magnitudes in different wavelength bands (labelled with corresponding letters) corrected from interstellar reddening. Predicted magnitudes from the isochrone part of our global model are shown as grey squares. The blue line is a theoretical spectra for a star with $T_{\text{eff}} = 6000$ K, $\log g = 4.5$ dex and $[M/H] = 0$; adopted from Coelho (2014).

the FEROS spectra), $\text{Li } 6708 \text{ EW} = 84 \pm 7 \text{ mÅ}$ and $B - V = 0.52 \pm 0.03$ (corrected from extinction), we recover a $1-\sigma$ age estimate of 340-715-1500 Myr. This is slightly higher than our previous estimate, but we note that BAFFLES uses an age posterior extending by default to 12 Gyr. Comparing to the star sample used in Morris (2020), belonging to well studied star clusters, TOI-4562’s photometric variability and rotation period are respectively larger and smaller than any stars of age 1 Gyr, therefore pointing at a younger age. Applying a conservative maximum age cut off of 1.5 Gyr to the age posterior when running BAFFLES yields a $1-\sigma$ age of 320-619-1100 Myr, closer to previously quoted values.

4. ANALYSIS AND RESULTS

To best determine the system properties of TOI-4562, we perform a joint modeling of all available photometric and spectroscopic datasets, including stellar isochrone models that constrain the properties of the host star. The paragraphs below detail individual components of this model.

4.1. Transit modeling

Despite the 225 day orbital period of TOI-4562 b, the extensive observations of TOI-4562 by *TESS* allowed four transits to be observed. Spot modulated variability at the $\sim 3\%$ level is seen on the *TESS* light curve due

to the active nature of TOI-4562, as expected given its young age. For the purposes of the transit modeling, we detrend the region around each transit epoch with a fourth-order polynomial. The polynomial is fitted using the out-of-transit regions of the light curve within 0.5 days of the transit center. We model the transits as per Mandel & Agol (2002) via the BATMAN package (Kreidberg 2015). Free parameters that describe the transit model include the transit centre T_c at each transit epoch, radius ratio R_p/R_* , line of sight inclination of the transit i , and the eccentricity parameters $\sqrt{e} \cos \omega$ and $\sqrt{e} \sin \omega$. A quadratic model was used to account for Limb Darkening using coefficients μ_{1TESS} and μ_{2TESS} fixed to those interpolated from Claret (2017) at the atmospheric parameters of TOI-4562 for the *TESS* transits. We note that a/R_* was not directly sampled but rather computed from the free parameters P_{orb} , M_* , R_* and planet mass M_p . For the two (same epoch, different telescopes) SAAO LCOGT transits, the Limb Darkening coefficients μ_{1LCO} and μ_{2LCO} are computed for the SDSS i' band from Claret & Bloemen (2011), using the interpolation routine from Eastman et al. (2013) with $T_{eff} = 6000$ K, $\log g = 4.5$ and $[M/H] = 0.1$, computed with the least square method (LSM). For the SAAO LCOGT data, we also incorporate the effects of instrumental systematic variations that are common to ground-based photometric observations via a simultaneous detrending of the light curve against parameters describing the observation airmass to which we add a linear trend with respect to time. All detrended light curves and the best transit model fits are shown in Figure 2.

4.2. Eccentric orbit validation

Even though the transit shape points to a very eccentric orbit, this can be degenerate with the mean stellar density ρ_* . To cross validate the eccentric nature of TOI-4562 b's orbit, we compared the stellar density obtained from isochrone fitting, which we call ρ_* , to the stellar density obtained from a forced circular orbit, that we call ρ_{circ} . To obtain ρ_{circ} , we run a transit only model, imposing $e = 0$ and with the following free parameters: ρ_{circ} , transit center T_c for each transits, radius ratio R_p/R_* , impact parameter b , limb darkening coefficients (μ_{1LCO} , μ_{2LCO} , μ_{1TESS} and μ_{2TESS}) and instrument systematics parameters (for the SAAO LCOGT transits). Leveraging this photo-eccentric effect (Dawson et al. 2012) allow us to recover the space of possible parameters for e and w (see Dawson et al. 2015). On Figure 8, we show in blue the resulting 2d distribution of e and w that agree with the derived ratio for ρ_{circ}/ρ_* ,

given¹:

$$\frac{\rho_{circ}}{\rho_*} = \frac{(1 + e \sin w)^3}{(1 - e^2)^{3/2}} \quad (1)$$

This grants us increased confidence of the true eccentric nature of TOI-4562 b's orbit.

4.3. Radial velocity modeling

The radial velocities obtained over the 2 consecutive orbits of TOI-4562 b were modeled using a Keplerian orbit. Some fitted parameters are shared with the transits and stellar isochrone fitting, such as T_c , P_{orb} , a/R_* (derived), R_* , M_* , i , $\sqrt{e} \cos \omega$ and $\sqrt{e} \sin \omega$. To model the velocities, we add the planet mass M_p , a radial velocity offset γ_{rel} , and a white noise term, σ_{Y1} . The semi-amplitude of the planetary signature K_{amp} was computed from the above parameters. The orbital solution and the associated likelihood from the fit to the data are computed from K_{amp} , T_c , P_{orb} , $\sqrt{e} \cos \omega$ and $\sqrt{e} \sin \omega$ via the RADVEL package (Fulton et al. 2018).

We also try to add a Gaussian Process using a Quasi-Periodic kernel, implemented through RADVEL to model the stellar noise apparent in the data. The resulting parameter values do not yield a significant difference, therefore not justifying the necessity to use a correlated noise model to account for the stellar intrinsic variability seen in the radial velocities. With one datapoint a day at most, the sampling is too sparse for the Gaussian Process to correctly grasp the ~ 4 days stellar period. Crudely assuming a spot covering 0.6-1.2% (δ_{spot}) of the stellar surface, we can approximate an activity induced radial velocity semi-amplitude K_{act} of $v \sin i \times \delta_{spot} \sim 100 - 200 \text{ m s}^{-1}$, comparable to the jitter level seen in Figure 4.

We attempted to fit a second longer period circular planet to the radial velocities. We used uniform priors for the period ($\mathcal{U}[300 : 2000]$ days), planet mass ($\mathcal{U}[0.002 : 0.1] M_\odot$) and t_0 ($\mathcal{U}[1398 : 3398]$ TBJD). The posterior distribution are not clearly converging, favouring larger periods and smaller masses. With a K_{amp} of $\sim 70 \text{ m s}^{-1}$, the best solution is clearly below the activity level and therefore not trustworthy. Long term data is needed to attempt to constrain a longer period companion.

4.4. Spectral energy distribution model

To constrain the host star parameters R_* , M_* , $[M/H]$ and T_{eff} we also model the spectral energy distribution of TOI-4562 simultaneously to the transit and

¹ In the case of TOI-4562 b, the condition $(\frac{a}{R_*})^2 \gg \frac{2}{3} \left(\frac{1+e}{1-e}\right)^3$, required for 1 to be valid (see Kipping 2014) is fulfilled.

radial velocity models. The stellar parameters are modeled using the MESA Isochrones & Stellar Tracks (Paxton et al. 2011, 2013, 2015; Choi et al. 2016). We interpolate evolution tracks using the MINIMINT package (Koposov 2021) against M_* , age, $[M/H]$ and the photometric bands B , V , $Gaia\ G$, Bp , Rp , 2MASS bands J , H , and K . R_* is derived from the isochrone predicted values for $\log g$ and M_* . To account for uncertainties in the stellar evolution models, we adopt a 4% uncertainty floor in stellar radius, and 5% floor in stellar mass, where appropriate (Tayar et al. 2022). For the effective temperature T_{eff} , we apply a Gaussian prior such that the predicted T_{eff} interpolated from the isochrone is compared against that measured from the CHIRON spectra as an additional likelihood term. Predicted fluxes from the SED model are corrected for interstellar reddening with the PYASTRONOMY UNRED package, that uses the parameterization from Fitzpatrick (1999). Extinction is a free parameter, with a maximum value of $E(B - V) = 0.1542$ mag, as estimated from the Schlafly & Finkbeiner (2011) maps over a 5 arcmin radius² around TOI-4562. We also incorporate a Gaussian prior on the distance modulus via the observed $Gaia$ parallax to TOI-4562. We offset $Gaia$ DR3’s parallax value by -0.023861 mas, the parallax zero-point offset estimated using the routine from Lindegren et al. (2021a)³ and function of ecliptic latitude, magnitude and colour. At each MCMC jump step, the observed spectral energy distribution is compared against the interpolated MIST model predictions for a given tested stellar parameter.

4.5. Global model

The global model includes simultaneous fits of the $TESS$ and ground-based photometric datasets (4.1), the CHIRON velocities (4.3), and stellar isochrone model (4.4), as shown in Figure 2, 4 and 7 respectively. We explore the best fit parameters and the posterior distribution via the Affine Invariant Markov chain Monte Carlo Ensemble sampler EMCEE (Foreman-Mackey et al. 2013). The resulting parameters for TOI-4562 b are given in Table 2.

Figure 8 illustrates the contribution of each part of the model to constrain the high eccentricity of TOI-4562 b. In blue we show the distribution stemming from the value of ρ_* when imposing a circular orbit to the planet and fitting only for transits (see Section 4.2). Then, a model containing both the transits and isochrones, shown in red, greatly constrain the eccentricity. Finally, the addition of RVs (shown in yellow) only slightly im-

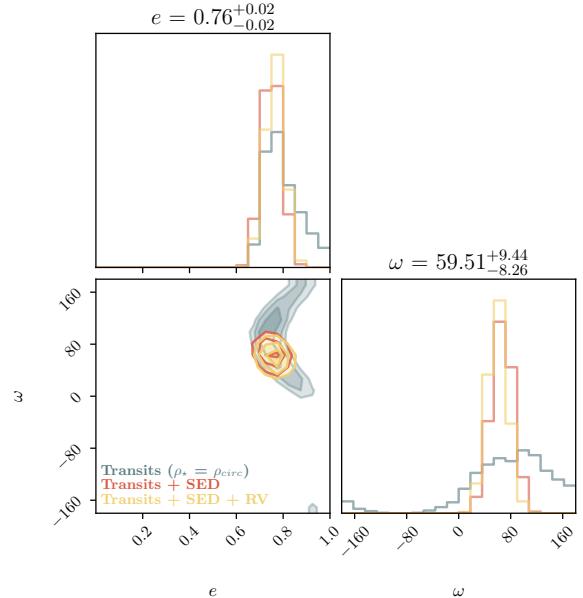


Figure 8. Posterior distributions for TOI-4562 b’s orbital eccentricity (e) and argument at periape (ω). The blue distribution was obtained from comparing ρ_* obtained from a SED fit and ρ_{circ} resulting from a fit of only the photometric data ($TESS$ + LCO-SAAO) with an imposed circular orbit. The red and yellow posterior distributions respectively results from a photometric data + SED fit and the complete model including the radial velocities.

proves the constrain the eccentricity, due to both the large stellar activity and the poor coverage of the periastron passages.

5. DISCUSSIONS AND CONCLUSIONS

We report the discovery of TOI-4562 b, a temperate gas giant on a highly eccentric orbit around a young Sun-like star. The planet has a mass of $2.30^{+0.48}_{-0.47} M_J$ and a radius of $1.118^{+0.014}_{-0.013} R_J$. With an orbital period of $225.11781^{+0.00025}_{-0.00022}$ days, it is to date the second longest period planet in the $TESS$ sample (after TOI-2180b, Dalba et al. 2022). TOI-4562 b’ resides in a highly elliptic orbit ($e=0.76^{+0.02}_{-0.02}$), and has, based on (Spada & Lanzafame 2020), an age younger than the Praesepe and Hyades clusters. A representation of its orbit alongside the inner Solar System planets is shown in Figure 9.

5.1. Radius evolution

At the end of their accretion phase, newly formed gas giants are expected to have radii larger than $1 R_J$. As the planet core radiates its primordial internal heat, Jovian mass planets will cool down via Kelvin-Helmholtz

² Obtained from the [NASA/IPAC Infrared Science Archive](https://archive.nasa.gov/)

³ https://gitlab.com/icc-ub/public/gaiadr3_zero_point

Table 2. TOI-4562 b parameters.

Parameters	Description	Priors	Values
Transit parameters			
$T_{c,1}^a$	Transit mid-time (BJD_{TDB})	$\mathcal{U}[1456.83, 1456.93]$	$1456.87991^{+0.00142}_{-0.00120}$
$T_{c,2}^a$	Transit mid-time (BJD_{TDB})	$\mathcal{U}[1681.94, 1682.04]$	$1681.98324^{+0.00136}_{-0.00142}$
$T_{c,3}^a$	Transit mid-time (BJD_{TDB})	$\mathcal{U}[2132.17, 2132.27]$	$2132.21577^{+0.00088}_{-0.00095}$
$T_{c,4}^a$	Transit mid-time (BJD_{TDB})	$\mathcal{U}[2357.29, 2357.39]$	$2357.34544^{+0.00079}_{-0.00080}$
$T_{c,5}^a$	Transit mid-time (BJD_{TDB})	$\mathcal{U}[2582.41, 2582.51]$	$2582.46321^{+0.00142}_{-0.00036}$
T_c^a	Derived linear ephemeris	$\mathcal{U}[1456.83, 1456.93]$	$1456.87168^{+0.00101}_{-0.00101}$
P_{orb}^a	Orbital period (days)	Derived linear ephemeris	$225.11781^{+0.00025}_{-0.00022}$
T_{14}	Transit total duration (hours)	-	4.32 ± 0.04
R_p/R_\star	Radius ratio	$\mathcal{U}[0, 0.2]$	$0.09980^{+0.00084}_{-0.00092}$
a/R_\star	Normalised Semi-major axis, derived from $[M_\star, R_\star, P_{\text{orb}}, M_p]$	-	$147.4^{+1.44}_{-1.26}$
b	Impact parameter	-	$0.60^{+0.03}_{-0.04}$
δ	Transit depth (ppm)	-	9961^{+167}_{-184}
$\sqrt{e} \cos \omega^a$	Reparameterization of e and ω	$\mathcal{U}[-1, 1]$	$0.442^{+0.110}_{-0.131}$
$\sqrt{e} \sin \omega^a$	Reparameterization of e and ω	$\mathcal{U}[-1, 1]$	$0.752^{+0.058}_{-0.063}$
i	Planet orbit inclination ($^\circ$)	$\mathcal{U}[84, 90]$	89.06 ± 0.04
$\mu_{1\text{TESS}}^b$	Quadratic Limb Darkening law coefficient 1 (TESS)	Fixed	0.28
$\mu_{2\text{TESS}}^b$	Quadratic Limb Darkening law coefficient 2 (TESS)	Fixed	0.29
$\mu_{1\text{LCO}}^c$	Quadratic Limb Darkening law coefficient 1 (LCO)	Fixed	0.28
$\mu_{2\text{LCO}}^c$	Quadratic Limb Darkening law coefficient 2 (LCO)	Fixed	0.29
Radial velocities parameters			
K	RV Semi-amplitude (ms^{-1})	-	106^{+24}_{-26}
M_p	Mass (M_\odot)	$\mathcal{U}[0, 0.2]$	0.0022 ± 0.0005
γ_{CHIRON}	RV offset (ms^{-1})	$\mathcal{U}[5200, 5400]$	5347 ± 13
σ_{Y1}	RV jitter, first orbit (ms^{-1})	$\mathcal{U}[0, 600]$	73^{+15}_{-15}
Derived parameters			
R_p	Radius (R_\oplus)	-	12.53 ± 0.15
	Radius (R_J)	-	$1.118^{+0.014}_{-0.013}$
M_p	Mass (M_\oplus)	-	732^{+152}_{-149}
	Mass (M_J)	-	$2.30^{+0.48}_{-0.47}$
e	Eccentricity	-	$0.76^{+0.02}_{-0.02}$
w	Argument at periape ($^\circ$)	-	60^{+9}_{-8}
ρ_p	Density (g cm^{-3})	-	$2.06^{+0.42}_{-0.44}$
a	Semi-major axis (AU)	-	$0.768^{+0.005}_{-0.005}$
$\langle T_{\text{eq}} \rangle$	Temporal average equilibrium temperature (K) ^d	-	318 ± 4
T_{peri}	Equilibrium temperature at periape (K)	-	717^{+29}_{-37}
T_{apo}	Equilibrium temperature at apoapsis (K)	-	262^{+3}_{-2}

Priors: $\mathcal{U}[a, b]$ uniform priors with boundaries a and b

^aParameters common to the Transit and RV models

^bAdopted at the *TESS* band from Claret (2017), using ATLAS model with $T_{\text{eff}} = 6000\text{K}$, $\log g = 4.5$ and $[M/H] = 0.1$ and computed with the least square method (LSM)

^cComputed for the SDSS *i'* band from Claret & Bloemen (2011), using the interpolation routine from Eastman et al. (2013) with $T_{\text{eff}} = 6000\text{K}$, $\log g = 4.5$ and $[M/H] = 0.1$ and computed with the least square method (LSM)

^dComputed for an elliptical orbit from Méndez & Rivera-Valentín (2017), using an albedo of $A = 0.4$, $\epsilon = 1$ and $\beta = 0.74$.

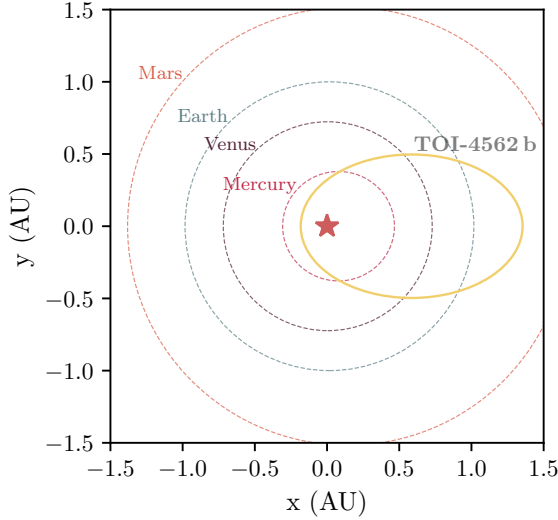


Figure 9. Two dimensional orbit of TOI-4562 b (yellow solid line) compared with Mercury (red dashed line), Venus (purple dashed line), Earth (blue dashed line) and Mars (orange dashed line).

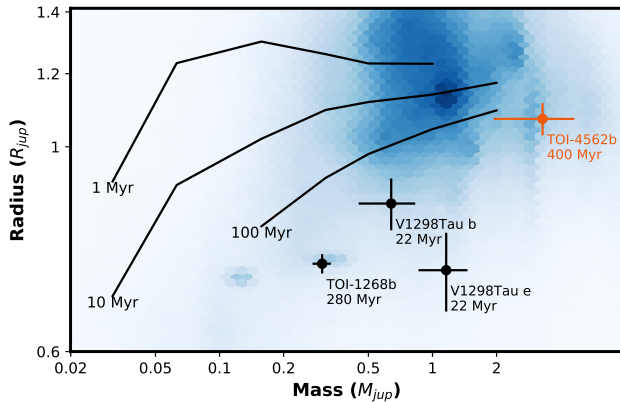


Figure 10. Young gas giants can help constrain the cooling and contraction models. To date, TOI-4562 b is only the fourth Jovian planet younger than 500 Myr to have both its mass and radius measured. The mass-radius of TOI-4562 b is plotted in orange alongside the planets in the V1298 Tau (David et al. 2019a; Suárez Mascareño et al. 2022) and TOI-1268 (Dong et al. 2022; Šubjak et al. 2022) systems. Unlike others, TOI-4562 b sits along the isochrone tracks that model the contraction of young planets (Linder et al. 2019). The mass-radius distribution of other known planets are shown with a density plot in blue in the background.

contraction to $\sim 1 R_J$. Only Hot Jupiters, orbiting extremely close to their parent star are expected to remain inflated due to their increased irradiation. According to cooling models (Baraffe et al. 2003; Fortney et al. 2007; Baraffe et al. 2008; Linder et al. 2019), shown on

Figure 10, the most drastic changes in radius occur at the earliest ages. Measuring radii of young gas giants like TOI-4562 b is therefore essential to set constraints on these such models, as emphasized in Fortney et al. (2007).

The current picture is unclear as the recently measured mass of V1298 Tau b & e (Suárez Mascareño et al. 2022) yield much denser planets than predicted at 20 Myr old and require dramatic heavy element enrichment to somewhat reconcile with cooling models (see Figure 10). Conversely, TOI-4562 b’s radius is as expected for its age. At the closest approach to its host star (~ 0.18 AU), it receives stellar irradiation of $\sim 9.3 \times 10^4 \text{ W m}^{-2}$, or ~ 68 times that of Earth. Although above the $\sim 1.6 \times 10^4 \text{ W m}^{-2}$ threshold to trigger inflation, given by Sestovic et al. (2018) for planets more massive than $2.5 M_J$, TOI-4562 b’s orbital eccentricity means this level of irradiation affects the planet for a very short fraction of the orbit, not sufficient to trigger radius inflation.

5.2. Dynamical history of TOI-4562 b and benefits of additional follow-up

In its current observed state, TOI-4562 b’s semi major axis and eccentricity (see Figure 11) are not in favour of a high eccentricity migration scenario as a circularization of its orbit would take orders of magnitudes longer than the age of the universe ($\tau_{circ} \sim 1 \times 10^7$ Gyr, Goldreich & Soter 1966). It is possible, however, that the planet is experiencing ongoing eccentricity cycles and we happen to be observing it at a lower eccentricity. Reduction of the star-planet distance at periastron at the eccentricity peak of such cycles might allow the circularization process to be triggered as described in Dong et al. (2014). Disk-planet interactions can in principle excite the eccentricity of the orbit (Duffell & Chiang 2015) but this is restricted to low ($e \lesssim 0.2$) values, as shown with the red area on Figure 11. Debras et al. (2021) proposed that migration inside wide gaps carved in protoplanetary disks could result in gas giants with eccentricities up to 0.4. This is still insufficient to explain the very high eccentricity from TOI-4562 b’s orbit.

Another possible scenario to account for TOI-4562 b’s very high eccentricity is in-situ formation (or alternatively, smooth disk migration), followed by excitation from a companion. This can occur via secular interactions, or slow angular momentum exchanges with another body located further out, either periodically through e.g., von Zeipel-Lidov-Kozai cycles (von Zeipel 1910; Lidov 1962; Kozai 1962; Naoz 2016; Nagasawa

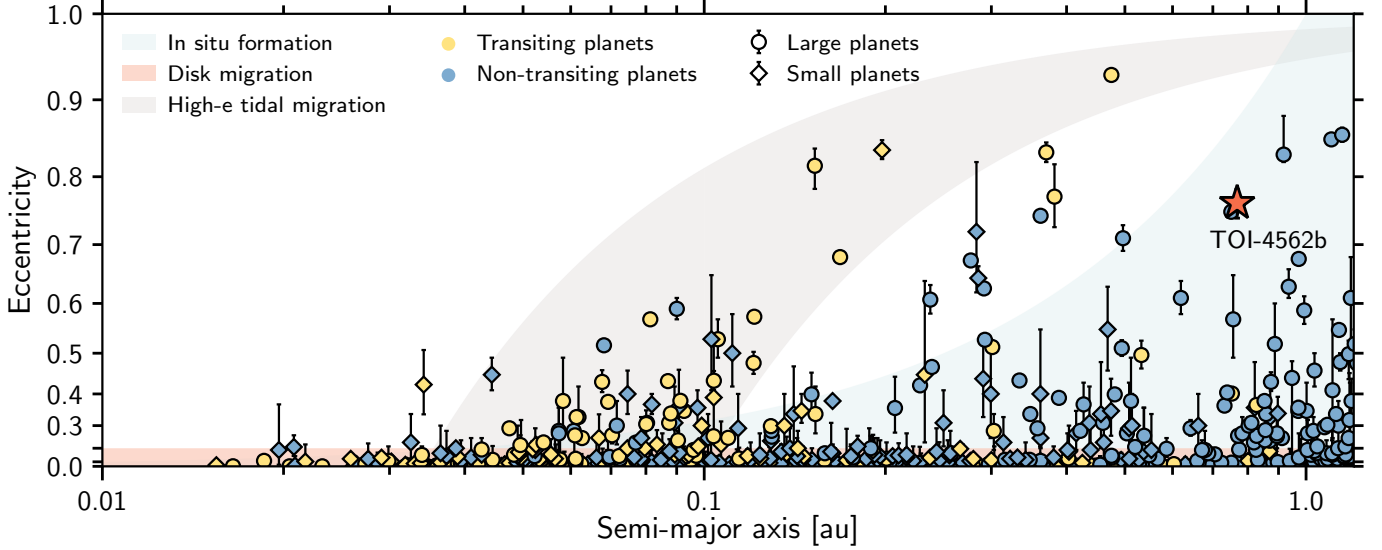


Figure 11. Eccentricity versus semi-major axis for all confirmed planets (Obtained from the NASA exoplanet archive 13 Feb. 2022) with $M_p < 13 M_J$. The vertical coordinate is scaled to e^2 to emphasize non-circular planets. Shaded areas highlight different formation scenarios. Planets in the grey region are on the path of high-eccentricity migration, with a final semi major axis between 0.034 and 0.1 au. The upper and lower bounds of this region are set by the Roche limit and the circularization timescale respectively. Disk migration, expected to only marginally excite orbital eccentricity is shown as the red shaded region. Finally, in situ formation, with eccentricity excited by, e.g., planet-planet scattering is shown in blue. Transiting versus non-transiting planets are labeled in yellow and blue respectively. Circles are representing larger ($R_p > 6 R_\oplus$ and/or $M_p > 100 M_\oplus$) planets and diamonds smaller planets ($R_p < 6 R_\oplus$ and/or $M_p < 100 M_\oplus$). Only planets with $e \geq 0.2$ and with uncertainties on e smaller than 50% of the measured e or planets with $e < 0.2$ and with uncertainties less than 0.2 are shown.

Table 3. Next 10 transit opportunities for TOI-4562b.

Transit mid-time (BJD)	Transit date	Visible from (Partial (P) or Full (F))	TESS simultaneity
2460032.6977	29-Mar-2023	Paranal (P)	Y
2460257.8142	9-Nov-2023	Paranal (P)	TBD
2460482.9307	21-Jun-2024	MKO (P) & ASTEP (F)	TBD
2460708.0473	1-Feb-2025	MKO (F)	TBD
2460933.1638	14-Sep-2025	MKO (P) & ASTEP (F)	TBD
2461158.2803	27-Apr-2026	SAAO (P) & RUN (P) & ASTEP (F)	TBD
2461383.3968	8-Dec-2026	SAAO (P) & RUN (F)	TBD
2461608.5134	27-Jul-2027	ASTEP (P)	TBD
2461833.6299	3-Mar-2028	SAAO (P) & Paranal (F)	TBD

Locations SAAO: South African Astronomical Observatory, South Africa (latitude = -32.379444, longitude = -339.189306), Paranal: European Southern Observatory at Paranal, Chile (latitude = -24.625, longitude = -70.403333), MKO: Mt. Kent Observatory, Australia (latitude = -27.797861, longitude = 151.855417), RUN: Observatoire astronomique des Makes, Reunion Island (latitude = -21.199359, longitude = 55.409464), ASTEP: Antarctic Search for Transiting ExoPlanets, Dome C, Antarctica (latitude = -75.09978, longitude = 123.332196)

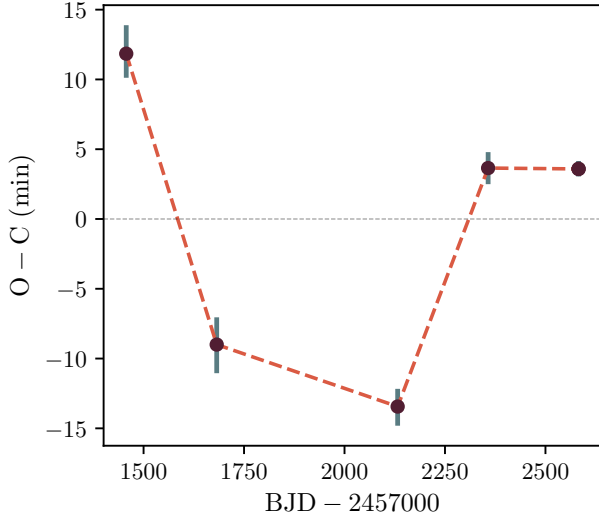


Figure 12. Observed - Calculated mid-transit time for the 5 transits of TOI-4562 b, in minutes. The second and third transits (from TESS Sectors 13 and 30) show a ~ 20 min mid-transit time difference with the other transits, suggesting the presence of a third body in the system.

et al. 2008) or chaotically in secular chaos (Wu & Lithwick 2011; Hamers et al. 2017). High eccentricity can also be triggered sporadically in planet-planet scattering (Weidenschilling & Marzari 1996; Rasio & Ford 1996; Ford & Rasio 2006; Chatterjee et al. 2008), or stellar fly-bys (Shara et al. 2016; Rodet et al. 2021). Planet-planet scattering could have happened quickly and potentially early if triggered by the dissipation of the gas disk or if the planets were initially closely spaced. Constraints on an outer companion (if not ejected as a result of scattering) could provide crucial insights on dynamical evolution timescales give the young age of the system.

The five transits of TOI-4562 b show modest deviation from a linear ephemeris fit on the 5 – 20 min level (see Figure 12). This potential detection of a transit timing variation signal suggests the presence of a companion in the system, to which TOI-4562 b probably owes its high eccentricity. The existing data are not sufficient to set meaningful constraints on the companion and most configurations for period (i.e., inner or outer companion), eccentricity and mutual inclination remain possible. TOI-4562 b will be observed by *TESS* again in its second extended mission in 2023. In Table 3, we show future opportunities to continue monitoring transits of TOI-4562 b in the years to come. Combining these with long-term radial velocity follow-up might enable us to unravel the 3-D architecture and dynamical history of this system, as has been successfully performed for

Kepler-419 b & c (Dawson et al. 2012, 2014). We also note that no transit duration variations were found.

The orbital astrometric motion of an outer companion could be retrieved from *Gaia* in the upcoming release of astrometric solutions for ~ 1.3 billion stars (Lindgren et al. 2021b). When archival Hipparchos and *Gaia* observations have been analysed jointly for previous brighter systems (e.g., Venner et al. 2021), astrometric accelerations have often yielded constraints for outer stellar massed companions to key exoplanet systems. Additional *Gaia* observations over the next ~ 10 years will allow us to achieve similar constraints for TOI-4562. Combined with the diffraction limited adaptive optics observations estimated to reach ~ 35 au (see section 2.5), these constraints can inform the presence of exterior stellar companions and provide means to distinguish between evolution scenarios.

Another candidate tracer for dynamical history is the angle between the star’s rotation axis and the planet’s orbital axis, or (sky projected) obliquity. From P_* , R_* and $v \sin i$, we estimate the stellar inclination with respect to the line of sight to have a 3σ lower bound of 70° as per Masuda & Winn (2020), consistent with being well aligned. Similarly to other planetary characteristics, the young (< 1 Gyr) end of the obliquity distribution is under sampled. Recent measurements resulting from *TESS* discoveries reveal a remarkable systematic alignment of young systems, including the Jupiter-sized planet HIP 67522 b (Rizzuto et al. 2020; Heitzmann et al. 2021), as well as a number of smaller planets (e.g., AU Mic b & c; Plavchan et al. (2020); Palle et al. (2020); Martioli et al. (2020); Hirano et al. (2020); Addison et al. (2021), DS Tuc Ab; Newton et al. (2019); Zhou et al. (2020); Montet et al. (2020), TOI 942 b & c Wirth et al. (2021), and TOI 251 Zhou et al. (2021)). The estimated amplitude of the Rossiter McLaughlin effect (Rossiter 1924; McLaughlin 1924) for TOI-4562 b is $\Delta V \sim 70\text{--}150 \text{ ms}^{-1}$. Given the ~ 4 hours transit duration, combined with a brightness of $V = 12.098$ and a rotational broadening of $v \sin i = 17.5 \text{ km s}^{-1}$, this is well within the grasp of a 4m-class telescope and such an eccentric system would provide a precious addition to the age-obliquity distribution. It is important to note that the long orbital period remains a major obstacle to transit spectroscopy for ground-based facilities.

In the coming years, we aim to conduct extensive follow-ups of the TOI-4562 system to unravel the full architecture of the system and potentially provide insights into the processes shaping the current gas giant planet distribution. Such follow-up will include radial velocities, ground and space based photometry, astrome-

try and transit spectroscopy for obliquity measurements and/or atmospheric characterisation.

We respectfully acknowledge the traditional custodians of the lands on which we conducted this research and throughout Australia. We recognize their continued cultural and spiritual connection to the land, waterways, cosmos and community. We pay our deepest respects to all Elders, present and emerging people of the Giabal, Jarowair and Kambuwal nations, upon whose lands the MINERVA-Australis facility at Mount Kent is located. This research has been supported by an Australian Government Research Training Program Scholarship. GZ thanks the support of the ARC DECRA program DE210101893. GZ, SQ thank the support of the *TESS* Guest Investigator Program G03007. CH thanks the support of the ARC DECRA program DE200101840. EG gratefully acknowledges support from the David and Claudia Harding Foundation in the form of a Winton Exoplanet Fellowship. This work was supported by an LSSTC Catalyst Fellowship awarded by LSST Corporation to TD with funding from the John Templeton Foundation grant ID # 62192. This research has used data from the CTIO/SMARTS 1.5m telescope, which is operated as part of the SMARTS Consortium by RECONS. This work has made use of data from the European Space Agency (ESA) mission *Gaia* (<https://www.cosmos.esa.int/gaia>), processed by the *Gaia* Data Processing and Analysis Consortium (DPAC, <https://www.cosmos.esa.int/web/gaia/dpac/consortium>). Funding for the DPAC has been provided by national institutions, in particular the institutions participating in the *Gaia* Multilateral Agreement. This work makes use of observations from the LCOGT network. Part of the LCOGT telescope time was granted by NOIRLab through the Mid-Scale Innovations Program (MSIP). MSIP is funded by NSF. This research has made use of the NASA Exoplanet Archive, which is operated by the California Institute of Technology, under contract with the National Aeronautics and Space Administration under the Exoplanet Exploration Program. Funding for the *TESS* mission is provided by NASA's Science Mission directorate. We acknowledge the use of public *TESS* Alert data from pipelines at the *TESS* Science Office and at the *TESS* Science Processing Operations Center. This research has made use of the Exoplanet Follow-up Observation Program website, which is operated by the California Institute of Technology, under contract with the National Aeronautics and Space Administration under the Exoplanet Exploration Program. This paper includes data collected by the *TESS* mission,

which are publicly available from the Mikulski Archive for Space Telescopes (MAST). Resources supporting this work were provided by the NASA High-End Computing (HEC) Program through the NASA Advanced Supercomputing (NAS) Division at Ames Research Center for the production of the SPOC data products. The Center for Exoplanets and Habitable Worlds is supported by the Pennsylvania State University and the Eberly College of Science. RB and MH acknowledge support from ANID – Millennium Science Initiative – ICN12.009. NE thanks everyone who takes part in the Planet Hunters *TESS* citizen science project, which contributes to finding new and exciting planetary systems.

Facility: *TESS*, Exoplanet Archive, CTIO 1.5 m, LCOGT, Gemini:Zorro, CTIO SOAR, ESO 2.2 m

Software: ASTROIMAGEJ (Collins et al. 2017), ASTROPY (Astropy Collaboration et al. 2013a, 2018a), BAFFLES (Stanford-Moore et al. 2020), BATMAN (Kreidberg 2015), CELERITE (Foreman-Mackey et al. 2017), EMCEE (Foreman-Mackey et al. 2013), PYASTRONOMY (Czesla et al. 2019), COMOVE (<https://github.com/adamkraus/Comove>), PYPHOT (<https://mfouesneau.github.io/pyphot/>), RADVEL (Fulton et al. 2018), SCIKIT-LEARN (Pedregosa et al. 2011), MINIMINT (<https://zenodo.org/record/4900576>), NUMPY (Harris et al. 2020), MATPLOTLIB (Hunter 2007), ASTROPY (Astropy Collaboration et al. 2013b, 2018b), UNRED (<https://github.com/pbrus/unreddden-stars>), PANDAS (pandas development team 2020), CORNER (Foreman-Mackey 2016)

Table 4. CHIRON radial velocities for TOI-4562. The two left columns cover TOI-4562 b's first orbit (late 2020 to mid 2021) and the two right columns the second orbit (late 2021 to early 2022).

BJD	RV (m s^{-1})	BJD	RV (m s^{-1})
2457919.279641	5362.7 ± 78.4	2457951.584780	5312.4 ± 84.9
2457919.975844	5384.0 ± 107.5	2457951.882422	5298.0 ± 99.8
2457920.077478	5338.8 ± 64.0	2457952.183280	5356.5 ± 69.2
2457920.770002	5472.3 ± 80.6	2457952.483116	5341.9 ± 81.1
2457923.866595	5150.9 ± 69.1	2457952.785734	5291.7 ± 116.4
2457924.163829	5375.4 ± 96.4	2457953.181198	5283.6 ± 75.4
2457926.463031	5361.0 ± 110.4	2457953.478271	5374.3 ± 68.4
2457926.769474	5386.8 ± 75.5	2457953.779370	5412.8 ± 62.9
2457927.459646	5307.2 ± 64.6	2457954.078933	5331.6 ± 90.0
2457927.755236	5311.9 ± 93.8	2457954.477875	5593.4 ± 68.6
2457928.059467	5417.3 ± 78.6	2457954.770163	5464.1 ± 66.4
2457928.466230	5204.1 ± 138.8	2457955.179212	5513.8 ± 94.8
2457928.761200	5199.1 ± 80.0	2457955.280537	5461.7 ± 89.2
2457929.259193	5241.1 ± 77.4	2457955.375845	5543.3 ± 92.6
2457929.558164	5370.1 ± 111.4	2457955.482781	5522.4 ± 82.3
2457929.953730	5152.4 ± 83.3	2457955.578297	5313.6 ± 101.5
2457930.253505	5155.4 ± 127.6	2457955.677910	5531.5 ± 77.8
2457930.457509	5435.7 ± 74.4	2457955.978882	5386.7 ± 76.3
2457930.752931	5245.4 ± 135.4	2457956.078722	5357.4 ± 49.4
2457931.049893	5485.1 ± 54.3	2457956.174936	5429.0 ± 78.6
2457931.459114	5335.7 ± 122.9	2457956.268873	5451.4 ± 128.8
2457931.852818	5329.3 ± 89.8	2457956.477261	5454.5 ± 88.7
2457932.354462	5475.9 ± 87.3	2457956.567821	5509.4 ± 74.6
2457932.753588	4941.1 ± 191.1	2457956.671976	5411.0 ± 75.6
2457932.950353	5350.4 ± 77.1	2457956.776594	5372.3 ± 78.1
2457933.157726	5182.6 ± 112.6	2457956.872101	5522.2 ± 121.3
2457933.548574	5679.6 ± 112.6	2457956.968008	5465.6 ± 120.6
2457934.251269	5352.0 ± 77.5	2457957.070850	5581.7 ± 80.9
2457934.548758	5707.1 ± 88.4	2457957.173735	5413.1 ± 59.1
2457934.949392	5777.3 ± 104.8	2457957.273394	5376.5 ± 83.0
2457935.148356	5684.9 ± 160.8	2457959.269741	5373.7 ± 120.7
2457935.644737	5348.6 ± 74.5	2457959.369361	5139.8 ± 94.1
2457935.744986	5126.8 ± 101.0	2457959.565821	5321.7 ± 74.9
2457936.045174	5124.1 ± 104.9	2457959.662741	5260.0 ± 81.5
2457936.146598	5314.9 ± 84.3	2457959.765341	5220.0 ± 60.7
2457936.345446	5322.3 ± 119.3	2457959.861135	5383.7 ± 87.1
2457936.438155	5581.4 ± 114.3	2457959.969637	5298.7 ± 108.3
2457936.545021	5093.0 ± 100.9	2457960.060741	5323.5 ± 60.7
2457936.646301	5255.5 ± 74.4	2457960.162519	5330.1 ± 87.7
2457936.744909	5271.4 ± 71.9	2457960.265488	5354.1 ± 53.1
2457936.846528	5428.8 ± 89.1	-	-
2457936.947656	5270.0 ± 69.6	-	-
2457937.046070	5415.1 ± 119.0	-	-
2457937.145298	5446.5 ± 132.6	-	-

REFERENCES

- Addison, B. C., Horner, J., Wittenmyer, R. A., et al. 2021, *AJ*, 162, 137, doi: [10.3847/1538-3881/ac1685](https://doi.org/10.3847/1538-3881/ac1685)
- Astropy Collaboration, Robitaille, T. P., Tollerud, E. J., et al. 2013a, *A&A*, 558, A33, doi: [10.1051/0004-6361/201322068](https://doi.org/10.1051/0004-6361/201322068)
- . 2013b, *A&A*, 558, A33, doi: [10.1051/0004-6361/201322068](https://doi.org/10.1051/0004-6361/201322068)
- Astropy Collaboration, Price-Whelan, A. M., Sipőcz, B. M., et al. 2018a, *AJ*, 156, 123, doi: [10.3847/1538-3881/aabc4f](https://doi.org/10.3847/1538-3881/aabc4f)
- Astropy Collaboration, Price-Whelan, A. M., Sipőcz, B. M., et al. 2018b, *aj*, 156, 123, doi: [10.3847/1538-3881/aabc4f](https://doi.org/10.3847/1538-3881/aabc4f)
- Baraffe, I., Chabrier, G., & Barman, T. 2008, *A&A*, 482, 315, doi: [10.1051/0004-6361:20079321](https://doi.org/10.1051/0004-6361:20079321)
- Baraffe, I., Chabrier, G., Barman, T. S., Allard, F., & Hauschildt, P. H. 2003, *A&A*, 402, 701, doi: [10.1051/0004-6361:20030252](https://doi.org/10.1051/0004-6361:20030252)
- Barnes, S. A. 2007, *ApJ*, 669, 1167, doi: [10.1086/519295](https://doi.org/10.1086/519295)
- Baruteau, C., Crida, A., Paardekoooper, S. J., et al. 2014, in *Protostars and Planets VI*, ed. H. Beuther, R. S. Klessen, C. P. Dullemond, & T. Henning, 667, doi: [10.2458/azu_uapress.9780816531240-ch029](https://doi.org/10.2458/azu_uapress.9780816531240-ch029)
- Batygin, K., & Stevenson, D. J. 2010, *ApJL*, 714, L238, doi: [10.1088/2041-8205/714/2/L238](https://doi.org/10.1088/2041-8205/714/2/L238)
- Bianchi, L., Shiao, B., & Thilker, D. 2017, *ApJS*, 230, 24, doi: [10.3847/1538-4365/aa7053](https://doi.org/10.3847/1538-4365/aa7053)
- Boisse, I., Moutou, C., Vidal-Madjar, A., et al. 2009, *A&A*, 495, 959, doi: [10.1051/0004-6361:200810648](https://doi.org/10.1051/0004-6361:200810648)
- Bouma, L. G., Hartman, J. D., Brahm, R., et al. 2020, *AJ*, 160, 239, doi: [10.3847/1538-3881/abb9ab](https://doi.org/10.3847/1538-3881/abb9ab)
- Bouma, L. G., Curtis, J. L., Masuda, K., et al. 2022a, *AJ*, 163, 121, doi: [10.3847/1538-3881/ac4966](https://doi.org/10.3847/1538-3881/ac4966)
- Bouma, L. G., Kerr, R., Curtis, J. L., et al. 2022b, *arXiv e-prints*, arXiv:2205.01112, <https://arxiv.org/abs/2205.01112>
- Bouma, L. G., Curtis, J. L., Masuda, K., et al. 2022, *The Astronomical Journal*, 163, 121, doi: [10.3847/1538-3881/ac4966](https://doi.org/10.3847/1538-3881/ac4966)
- Bouvier, J., Barrado, D., Moraux, E., et al. 2018, *A&A*, 613, A63, doi: [10.1051/0004-6361/201731881](https://doi.org/10.1051/0004-6361/201731881)
- Brahm, R., Jordán, A., & Espinoza, N. 2017a, *PASP*, 129, 034002, doi: [10.1088/1538-3873/aa5455](https://doi.org/10.1088/1538-3873/aa5455)
- Brahm, R., Jordán, A., Hartman, J., & Bakos, G. 2017b, *MNRAS*, 467, 971, doi: [10.1093/mnras/stx144](https://doi.org/10.1093/mnras/stx144)
- Brown, T. M., Baliber, N., Bianco, F. B., et al. 2013, *PASP*, 125, 1031, doi: [10.1086/673168](https://doi.org/10.1086/673168)
- Buchhave, L. A., Latham, D. W., Johansen, A., et al. 2012, *Nature*, 486, 375, doi: [10.1038/nature11121](https://doi.org/10.1038/nature11121)
- Buder, S., Sharma, S., Kos, J., et al. 2021, *MNRAS*, 506, 150, doi: [10.1093/mnras/stab1242](https://doi.org/10.1093/mnras/stab1242)
- Castelli, F., & Kurucz, R. L. 2004, *ArXiv Astrophysics e-prints*
- Chabrier, G., Johansen, A., Janson, M., & Rafikov, R. 2014, in *Protostars and Planets VI*, ed. H. Beuther, R. S. Klessen, C. P. Dullemond, & T. Henning, 619, doi: [10.2458/azu_uapress.9780816531240-ch027](https://doi.org/10.2458/azu_uapress.9780816531240-ch027)
- Chatterjee, S., Ford, E. B., Matsumura, S., & Rasio, F. A. 2008, *ApJ*, 686, 580, doi: [10.1086/590227](https://doi.org/10.1086/590227)
- Choi, J., Dotter, A., Conroy, C., et al. 2016, *ApJ*, 823, 102, doi: [10.3847/0004-637X/823/2/102](https://doi.org/10.3847/0004-637X/823/2/102)
- Claret, A. 2017, *A&A*, 600, A30, doi: [10.1051/0004-6361/201629705](https://doi.org/10.1051/0004-6361/201629705)
- Claret, A., & Bloemen, S. 2011, *A&A*, 529, A75, doi: [10.1051/0004-6361/201116451](https://doi.org/10.1051/0004-6361/201116451)
- Coelho, P. R. T. 2014, *MNRAS*, 440, 1027, doi: [10.1093/mnras/stu365](https://doi.org/10.1093/mnras/stu365)
- Collins, K. A., Kielkopf, J. F., Stassun, K. G., & Hessman, F. V. 2017, *AJ*, 153, 77, doi: [10.3847/1538-3881/153/2/77](https://doi.org/10.3847/1538-3881/153/2/77)
- Cummings, J. D., Deliyannis, C. P., Maderak, R. M., & Steinhauer, A. 2017, *AJ*, 153, 128, doi: [10.3847/1538-3881/aa5b86](https://doi.org/10.3847/1538-3881/aa5b86)
- Curtis, J. L., Agüeros, M. A., Douglas, S. T., & Meibom, S. 2019, *ApJ*, 879, 49, doi: [10.3847/1538-4357/ab2393](https://doi.org/10.3847/1538-4357/ab2393)
- Cutri, R. M., Wright, E. L., Conrow, T., et al. 2021, *VizieR Online Data Catalog*, II/328
- Czesla, S., Schröter, S., Schneider, C. P., et al. 2019, *PyA: Python astronomy-related packages*, <http://ascl.net/1906.010>
- Dalba, P. A., Kane, S. R., Dragomir, D., et al. 2022, *AJ*, 163, 61, doi: [10.3847/1538-3881/ac415b](https://doi.org/10.3847/1538-3881/ac415b)
- David, T. J., Petigura, E. A., Luger, R., et al. 2019a, *ApJL*, 885, L12, doi: [10.3847/2041-8213/ab4c99](https://doi.org/10.3847/2041-8213/ab4c99)
- David, T. J., Cody, A. M., Hedges, C. L., et al. 2019b, *AJ*, 158, 79, doi: [10.3847/1538-3881/ab290f](https://doi.org/10.3847/1538-3881/ab290f)
- Dawson, R. I., & Johnson, J. A. 2018, *ARA&A*, 56, 175, doi: [10.1146/annurev-astro-081817-051853](https://doi.org/10.1146/annurev-astro-081817-051853)
- Dawson, R. I., Johnson, J. A., Morton, T. D., et al. 2012, *ApJ*, 761, 163, doi: [10.1088/0004-637X/761/2/163](https://doi.org/10.1088/0004-637X/761/2/163)
- Dawson, R. I., Murray-Clay, R. A., & Johnson, J. A. 2015, *ApJ*, 798, 66, doi: [10.1088/0004-637X/798/2/66](https://doi.org/10.1088/0004-637X/798/2/66)
- Dawson, R. I., Johnson, J. A., Fabrycky, D. C., et al. 2014, *ApJ*, 791, 89, doi: [10.1088/0004-637X/791/2/89](https://doi.org/10.1088/0004-637X/791/2/89)
- Debras, F., Baruteau, C., & Donati, J.-F. 2021, *MNRAS*, 500, 1621, doi: [10.1093/mnras/staa3397](https://doi.org/10.1093/mnras/staa3397)
- Dong, J., Huang, C. X., Zhou, G., et al. 2022, *ApJL*, 926, L7, doi: [10.3847/2041-8213/ac4da0](https://doi.org/10.3847/2041-8213/ac4da0)

- Dong, S., Katz, B., & Socrates, A. 2014, *ApJL*, 781, L5, doi: [10.1088/2041-8205/781/1/L5](https://doi.org/10.1088/2041-8205/781/1/L5)
- Douglas, S. T., Agüeros, M. A., Covey, K. R., et al. 2016, *ApJ*, 822, 47, doi: [10.3847/0004-637X/822/1/47](https://doi.org/10.3847/0004-637X/822/1/47)
- Douglas, S. T., Curtis, J. L., Agüeros, M. A., et al. 2019, *ApJ*, 879, 100, doi: [10.3847/1538-4357/ab2468](https://doi.org/10.3847/1538-4357/ab2468)
- Duffell, P. C., & Chiang, E. 2015, *ApJ*, 812, 94, doi: [10.1088/0004-637X/812/2/94](https://doi.org/10.1088/0004-637X/812/2/94)
- Duncan, D. K., Vaughan, A. H., Wilson, O. C., et al. 1991, *ApJS*, 76, 383, doi: [10.1086/191572](https://doi.org/10.1086/191572)
- Eastman, J., Gaudi, B. S., & Agol, E. 2013, *PASP*, 125, 83, doi: [10.1086/669497](https://doi.org/10.1086/669497)
- Fitzpatrick, E. L. 1999, *PASP*, 111, 63, doi: [10.1086/316293](https://doi.org/10.1086/316293)
- Ford, E. B., & Rasio, F. A. 2006, *ApJL*, 638, L45, doi: [10.1086/500734](https://doi.org/10.1086/500734)
- Foreman-Mackey, D. 2016, *JOSS*, 1, 24, doi: [10.21105/joss.00024](https://doi.org/10.21105/joss.00024)
- Foreman-Mackey, D., Agol, E., Angus, R., & Ambikasaran, S. 2017, *ArXiv*. <https://arxiv.org/abs/1703.09710>
- Foreman-Mackey, D., Hogg, D. W., Lang, D., & Goodman, J. 2013, *PASP*, 125, 306, doi: [10.1086/670067](https://doi.org/10.1086/670067)
- Fortney, J. J., Marley, M. S., & Barnes, J. W. 2007, *ApJ*, 659, 1661, doi: [10.1086/512120](https://doi.org/10.1086/512120)
- Fulton, B. J., Petigura, E. A., Blunt, S., & Sinukoff, E. 2018, *PASP*, 130, 044504, doi: [10.1088/1538-3873/aaaaa8](https://doi.org/10.1088/1538-3873/aaaaa8)
- Gagné, J., Mamajek, E. E., Malo, L., et al. 2018, *ApJ*, 856, 23, doi: [10.3847/1538-4357/aaae09](https://doi.org/10.3847/1538-4357/aaae09)
- Gaia Collaboration, Prusti, T., de Bruijne, J. H. J., et al. 2016, *A&A*, 595, A1, doi: [10.1051/0004-6361/201629272](https://doi.org/10.1051/0004-6361/201629272)
- Gaia Collaboration, Brown, A. G. A., Vallenari, A., et al. 2021, *A&A*, 649, A1, doi: [10.1051/0004-6361/202039657](https://doi.org/10.1051/0004-6361/202039657)
- Gillen, E., Briegal, J. T., Hodgkin, S. T., et al. 2020, *MNRAS*, 492, 1008, doi: [10.1093/mnras/stz3251](https://doi.org/10.1093/mnras/stz3251)
- Goldreich, P., & Soter, S. 1966, *Icarus*, 5, 375, doi: [10.1016/0019-1035\(66\)90051-0](https://doi.org/10.1016/0019-1035(66)90051-0)
- Guerrero, N. M., Seager, S., Huang, C. X., et al. 2021, *ApJS*, 254, 39, doi: [10.3847/1538-4365/abefel](https://doi.org/10.3847/1538-4365/abefel)
- Guillot, T., & Showman, A. P. 2002, *A&A*, 385, 156, doi: [10.1051/0004-6361:20011624](https://doi.org/10.1051/0004-6361:20011624)
- Guillot, T., Abe, L., Agabi, A., et al. 2015, *Astronomische Nachrichten*, 336, 638, doi: [10.1002/asna.201512174](https://doi.org/10.1002/asna.201512174)
- Hamers, A. S., Antonini, F., Lithwick, Y., Perets, H. B., & Portegies Zwart, S. F. 2017, *MNRAS*, 464, 688, doi: [10.1093/mnras/stw2370](https://doi.org/10.1093/mnras/stw2370)
- Harris, C. R., Millman, K. J., van der Walt, S. J., et al. 2020, *Nature*, 585, 357, doi: [10.1038/s41586-020-2649-2](https://doi.org/10.1038/s41586-020-2649-2)
- Heitzmann, A., Zhou, G., Quinn, S. N., et al. 2021, *ApJL*, 922, L1, doi: [10.3847/2041-8213/ac3485](https://doi.org/10.3847/2041-8213/ac3485)
- Henden, A. A., Templeton, M., Terrell, D., et al. 2016, *VizieR Online Data Catalog*, II/336
- Hirano, T., Krishnamurthy, V., Gaidos, E., et al. 2020, *ApJL*, 899, L13, doi: [10.3847/2041-8213/aba6eb](https://doi.org/10.3847/2041-8213/aba6eb)
- Howell, S. B., Everett, M. E., Sherry, W., Horch, E., & Ciardi, D. R. 2011, *AJ*, 142, 19, doi: [10.1088/0004-6256/142/1/19](https://doi.org/10.1088/0004-6256/142/1/19)
- Howell, S. B., & Furlan, E. 2022, *Frontiers in Astronomy and Space Sciences*, 9, 871163, doi: [10.3389/fspas.2022.871163](https://doi.org/10.3389/fspas.2022.871163)
- Huang, C. X., Vanderburg, A., Pál, A., et al. 2020, *Research Notes of the American Astronomical Society*, 4, 204, doi: [10.3847/2515-5172/abca2e](https://doi.org/10.3847/2515-5172/abca2e)
- Hunter, J. D. 2007, *Computing in Science & Engineering*, 9, 90, doi: [10.1109/MCSE.2007.55](https://doi.org/10.1109/MCSE.2007.55)
- Jayasinghe, T., Stanek, K. Z., Kochanek, C. S., et al. 2019, *MNRAS*, 485, 961, doi: [10.1093/mnras/stz444](https://doi.org/10.1093/mnras/stz444)
- Jenkins, J. M. 2002, *ApJ*, 575, 493, doi: [10.1086/341136](https://doi.org/10.1086/341136)
- Jenkins, J. M., Tenenbaum, P., Seader, S., et al. 2020, *Kepler Data Processing Handbook: Transiting Planet Search*, Kepler Science Document KSCI-19081-003
- Jenkins, J. M., Chandrasekaran, H., McCauliff, S. D., et al. 2010, in *Society of Photo-Optical Instrumentation Engineers (SPIE) Conference Series*, Vol. 7740, *Software and Cyberinfrastructure for Astronomy*, ed. N. M. Radziwill & A. Bridger, 77400D, doi: [10.1117/12.856764](https://doi.org/10.1117/12.856764)
- Jenkins, J. M., Twicken, J. D., McCauliff, S., et al. 2016, in *Proc. SPIE*, Vol. 9913, *Software and Cyberinfrastructure for Astronomy IV*, 99133E, doi: [10.1117/12.2233418](https://doi.org/10.1117/12.2233418)
- Kaufer, A., Stahl, O., Tubbesing, S., et al. 1999, *The Messenger*, 95, 8
- Kipping, D. M. 2014, *MNRAS*, 440, 2164, doi: [10.1093/mnras/stu318](https://doi.org/10.1093/mnras/stu318)
- Koposov, S. 2021, *segsai/minimint: Minimint 0.3.0, v0.3.0*, Zenodo, doi: [10.5281/zenodo.5610692](https://doi.org/10.5281/zenodo.5610692)
- Kounkel, M., & Covey, K. 2019, *AJ*, 158, 122, doi: [10.3847/1538-3881/ab339a](https://doi.org/10.3847/1538-3881/ab339a)
- Kovács, G., Zucker, S., & Mazeh, T. 2002, *A&A*, 391, 369, doi: [10.1051/0004-6361:20020802](https://doi.org/10.1051/0004-6361:20020802)
- Kozai, Y. 1962, *AJ*, 67, 591, doi: [10.1086/108790](https://doi.org/10.1086/108790)
- Kreidberg, L. 2015, *PASP*, 127, 1161, doi: [10.1086/683602](https://doi.org/10.1086/683602)
- Lanza, A. F., Rodono, M., & Zappala, R. A. 1993, *A&A*, 269, 351
- Li, J., Tenenbaum, P., Twicken, J. D., et al. 2019, *PASP*, 131, 024506, doi: [10.1088/1538-3873/aaf44d](https://doi.org/10.1088/1538-3873/aaf44d)
- Lidov, M. L. 1962, *Planet. Space Sci.*, 9, 719, doi: [10.1016/0032-0633\(62\)90129-0](https://doi.org/10.1016/0032-0633(62)90129-0)
- Lindgren, L., Bastian, U., Biermann, M., et al. 2021a, *A&A*, 649, A4, doi: [10.1051/0004-6361/202039653](https://doi.org/10.1051/0004-6361/202039653)
- Lindgren, L., Klioner, S. A., Hernández, J., et al. 2021b, *A&A*, 649, A2, doi: [10.1051/0004-6361/202039709](https://doi.org/10.1051/0004-6361/202039709)

- Linder, E. F., Mordasini, C., Mollière, P., et al. 2019, *A&A*, 623, A85, doi: [10.1051/0004-6361/201833873](https://doi.org/10.1051/0004-6361/201833873)
- Lomb, N. R. 1976, *Ap&SS*, 39, 447, doi: [10.1007/BF00648343](https://doi.org/10.1007/BF00648343)
- Mamajek, E. E., & Hillenbrand, L. A. 2008, *ApJ*, 687, 1264, doi: [10.1086/591785](https://doi.org/10.1086/591785)
- Mandel, K., & Agol, E. 2002, *ApJL*, 580, L171, doi: [10.1086/345520](https://doi.org/10.1086/345520)
- Mann, A. W., Johnson, M. C., Vanderburg, A., et al. 2020, *AJ*, 160, 179, doi: [10.3847/1538-3881/abae64](https://doi.org/10.3847/1538-3881/abae64)
- Mann, A. W., Wood, M. L., Schmidt, S. P., et al. 2021, arXiv e-prints, arXiv:2110.09531, <https://arxiv.org/abs/2110.09531>
- Martoli, E., Hébrard, G., Moutou, C., et al. 2020, *A&A*, 641, L1, doi: [10.1051/0004-6361/202038695](https://doi.org/10.1051/0004-6361/202038695)
- Masuda, K., & Winn, J. N. 2020, *AJ*, 159, 81, doi: [10.3847/1538-3881/ab65be](https://doi.org/10.3847/1538-3881/ab65be)
- McCully, C., Volgenau, N. H., Harbeck, D.-R., et al. 2018, in *Society of Photo-Optical Instrumentation Engineers (SPIE) Conference Series*, Vol. 10707, Proc. SPIE, 107070K, doi: [10.1117/12.2314340](https://doi.org/10.1117/12.2314340)
- McLaughlin, D. B. 1924, *ApJ*, 60, 22, doi: [10.1086/142826](https://doi.org/10.1086/142826)
- Meibom, S., Barnes, S. A., Platais, I., et al. 2015, *Nature*, 517, 589, doi: [10.1038/nature14118](https://doi.org/10.1038/nature14118)
- Mékarnia, D., Guillot, T., Rivet, J. P., et al. 2016, *MNRAS*, 463, 45, doi: [10.1093/mnras/stw1934](https://doi.org/10.1093/mnras/stw1934)
- Méndez, A., & Rivera-Valentín, E. G. 2017, *ApJL*, 837, L1, doi: [10.3847/2041-8213/aa5f13](https://doi.org/10.3847/2041-8213/aa5f13)
- Messina, S., Nardiello, D., Desidera, S., et al. 2022, *A&A*, 657, L3, doi: [10.1051/0004-6361/202142276](https://doi.org/10.1051/0004-6361/202142276)
- Montet, B. T., Feinstein, A. D., Luger, R., et al. 2020, *AJ*, 159, 112, doi: [10.3847/1538-3881/ab6d6d](https://doi.org/10.3847/1538-3881/ab6d6d)
- Morris, B. M. 2020, *ApJ*, 893, 67, doi: [10.3847/1538-4357/ab79a0](https://doi.org/10.3847/1538-4357/ab79a0)
- Morris, R. L., Twicken, J. D., Smith, J. C., et al. 2020, *Kepler Data Processing Handbook: Photometric Analysis*, *Kepler Data Processing Handbook (KSCI-19081-003)*
- Nagasawa, M., Ida, S., & Bessho, T. 2008, *ApJ*, 678, 498, doi: [10.1086/529369](https://doi.org/10.1086/529369)
- Nagasawa, M., Lin, D. N. C., & Ida, S. 2003, *ApJ*, 586, 1374, doi: [10.1086/367884](https://doi.org/10.1086/367884)
- Naoz, S. 2016, *ARA&A*, 54, 441, doi: [10.1146/annurev-astro-081915-023315](https://doi.org/10.1146/annurev-astro-081915-023315)
- Newton, E. R., Mann, A. W., Tofflemire, B. M., et al. 2019, *ApJL*, 880, L17, doi: [10.3847/2041-8213/ab2988](https://doi.org/10.3847/2041-8213/ab2988)
- Newton, E. R., Rampalli, R., Kraus, A. L., et al. 2022, arXiv e-prints, arXiv:2206.06254, <https://arxiv.org/abs/2206.06254>
- Noyes, R. W., Hartmann, L. W., Baliunas, S. L., Duncan, D. K., & Vaughan, A. H. 1984, *ApJ*, 279, 763, doi: [10.1086/161945](https://doi.org/10.1086/161945)
- Oh, S., Price-Whelan, A. M., Hogg, D. W., Morton, T. D., & Spergel, D. N. 2017, *AJ*, 153, 257, doi: [10.3847/1538-3881/aa6ffd](https://doi.org/10.3847/1538-3881/aa6ffd)
- Palle, E., Oshagh, M., Casasayas-Barris, N., et al. 2020, *A&A*, 643, A25, doi: [10.1051/0004-6361/202038583](https://doi.org/10.1051/0004-6361/202038583)
- pandas development team, T. 2020, *pandas-dev/pandas: Pandas, latest*, Zenodo, doi: [10.5281/zenodo.3509134](https://doi.org/10.5281/zenodo.3509134)
- Paredes, L. A., Henry, T. J., Quinn, S. N., et al. 2021, *AJ*, 162, 176, doi: [10.3847/1538-3881/ac082a](https://doi.org/10.3847/1538-3881/ac082a)
- Paxton, B., Bildsten, L., Dotter, A., et al. 2011, *ApJS*, 192, 3, doi: [10.1088/0067-0049/192/1/3](https://doi.org/10.1088/0067-0049/192/1/3)
- Paxton, B., Cantiello, M., Arras, P., et al. 2013, *ApJS*, 208, 4, doi: [10.1088/0067-0049/208/1/4](https://doi.org/10.1088/0067-0049/208/1/4)
- Paxton, B., Marchant, P., Schwab, J., et al. 2015, *ApJS*, 220, 15, doi: [10.1088/0067-0049/220/1/15](https://doi.org/10.1088/0067-0049/220/1/15)
- Pedregosa, F., Varoquaux, G., Gramfort, A., et al. 2011, *Journal of Machine Learning Research*, 12, 2825
- Plavchan, P., Barclay, T., Gagné, J., et al. 2020, *Nature*, 582, 497, doi: [10.1038/s41586-020-2400-z](https://doi.org/10.1038/s41586-020-2400-z)
- Pollacco, D. L., Skillen, I., Collier Cameron, A., et al. 2006, *PASP*, 118, 1407, doi: [10.1086/508556](https://doi.org/10.1086/508556)
- Rasio, F. A., & Ford, E. B. 1996, *Science*, 274, 954, doi: [10.1126/science.274.5289.954](https://doi.org/10.1126/science.274.5289.954)
- Rauer, H., Catala, C., Aerts, C., et al. 2014, *Experimental Astronomy*, 38, 249, doi: [10.1007/s10686-014-9383-4](https://doi.org/10.1007/s10686-014-9383-4)
- Rebull, L. M., Stauffer, J. R., Bouvier, J., et al. 2016, *AJ*, 152, 113, doi: [10.3847/0004-6256/152/5/113](https://doi.org/10.3847/0004-6256/152/5/113)
- Reinhold, T., Reiners, A., & Basri, G. 2013, *A&A*, 560, A4, doi: [10.1051/0004-6361/201321970](https://doi.org/10.1051/0004-6361/201321970)
- Ricker, G. R., Winn, J. N., Vanderspek, R., et al. 2015, *Journal of Astronomical Telescopes, Instruments, and Systems*, 1, 014003, doi: [10.1117/1.JATIS.1.1.014003](https://doi.org/10.1117/1.JATIS.1.1.014003)
- Rizzuto, A. C., Newton, E. R., Mann, A. W., et al. 2020, *AJ*, 160, 33, doi: [10.3847/1538-3881/ab94b7](https://doi.org/10.3847/1538-3881/ab94b7)
- Rodet, L., Su, Y., & Lai, D. 2021, *ApJ*, 913, 104, doi: [10.3847/1538-4357/abf8a7](https://doi.org/10.3847/1538-4357/abf8a7)
- Rossiter, R. A. 1924, *ApJ*, 60, 15, doi: [10.1086/142825](https://doi.org/10.1086/142825)
- Scargle, J. D. 1982, *ApJ*, 263, 835, doi: [10.1086/160554](https://doi.org/10.1086/160554)
- Schlafly, E. F., & Finkbeiner, D. P. 2011, *ApJ*, 737, 103, doi: [10.1088/0004-637X/737/2/103](https://doi.org/10.1088/0004-637X/737/2/103)
- Sestovic, M., Demory, B.-O., & Queloz, D. 2018, *A&A*, 616, A76, doi: [10.1051/0004-6361/201731454](https://doi.org/10.1051/0004-6361/201731454)
- Shappee, B., Prieto, J., Stanek, K. Z., et al. 2014, in *American Astronomical Society Meeting Abstracts*, Vol. 223, American Astronomical Society Meeting Abstracts #223, 236.03

- Shara, M. M., Hurley, J. R., & Mardling, R. A. 2016, *ApJ*, 816, 59, doi: [10.3847/0004-637X/816/2/59](https://doi.org/10.3847/0004-637X/816/2/59)
- Skrutskie, M. F., Cutri, R. M., Stiening, R., et al. 2006, *AJ*, 131, 1163, doi: [10.1086/498708](https://doi.org/10.1086/498708)
- Soderblom, D. R. 2010, *ARA&A*, 48, 581, doi: [10.1146/annurev-astro-081309-130806](https://doi.org/10.1146/annurev-astro-081309-130806)
- Spada, F., & Lanzafame, A. C. 2020, *A&A*, 636, A76, doi: [10.1051/0004-6361/201936384](https://doi.org/10.1051/0004-6361/201936384)
- Stanford-Moore, S. A., Nielsen, E. L., De Rosa, R. J., Macintosh, B., & Czekala, I. 2020, *ApJ*, 898, 27, doi: [10.3847/1538-4357/ab9a35](https://doi.org/10.3847/1538-4357/ab9a35)
- Stassun, K. G., Oelkers, R. J., Pepper, J., et al. 2018, *AJ*, 156, 102, doi: [10.3847/1538-3881/aad050](https://doi.org/10.3847/1538-3881/aad050)
- Suárez Mascareño, A., Damasso, M., Lodieu, N., et al. 2022, *Nature Astronomy*, 6, 232, doi: [10.1038/s41550-021-01533-7](https://doi.org/10.1038/s41550-021-01533-7)
- Tayar, J., Claytor, Z. R., Huber, D., & van Saders, J. 2022, *ApJ*, 927, 31, doi: [10.3847/1538-4357/ac4bbc](https://doi.org/10.3847/1538-4357/ac4bbc)
- Tofflemire, B. M., Rizzuto, A. C., Newton, E. R., et al. 2021, *AJ*, 161, 171, doi: [10.3847/1538-3881/abdf53](https://doi.org/10.3847/1538-3881/abdf53)
- Tokovinin, A. 2018, *PASP*, 130, 035002, doi: [10.1088/1538-3873/aaa7d9](https://doi.org/10.1088/1538-3873/aaa7d9)
- Tokovinin, A., Fischer, D. A., Bonati, M., et al. 2013, *PASP*, 125, 1336, doi: [10.1086/674012](https://doi.org/10.1086/674012)
- Twicken, J. D., Clarke, B. D., Bryson, S. T., et al. 2010, in *Proc. SPIE*, Vol. 7740, *Software and Cyberinfrastructure for Astronomy*, 774023, doi: [10.1117/12.856790](https://doi.org/10.1117/12.856790)
- Twicken, J. D., Catanzarite, J. H., Clarke, B. D., et al. 2018, *PASP*, 130, 064502, doi: [10.1088/1538-3873/aab694](https://doi.org/10.1088/1538-3873/aab694)
- Ujjwal, K., Kartha, S. S., Mathew, B., Manoj, P., & Narang, M. 2020, *AJ*, 159, 166, doi: [10.3847/1538-3881/ab76d6](https://doi.org/10.3847/1538-3881/ab76d6)
- Vanderburg, A., & Johnson, J. A. 2014, *PASP*, 126, 948, doi: [10.1086/678764](https://doi.org/10.1086/678764)
- Venner, A., Vanderburg, A., & Pearce, L. A. 2021, *AJ*, 162, 12, doi: [10.3847/1538-3881/abf932](https://doi.org/10.3847/1538-3881/abf932)
- von Zeipel, H. 1910, *Astronomische Nachrichten*, 183, 345, doi: [10.1002/asna.19091832202](https://doi.org/10.1002/asna.19091832202)
- Šubjak, J., Endl, M., Chaturvedi, P., et al. 2022, *arXiv e-prints*, arXiv:2201.13341, <https://arxiv.org/abs/2201.13341>
- Weidenschilling, S. J., & Marzari, F. 1996, *Nature*, 384, 619, doi: [10.1038/384619a0](https://doi.org/10.1038/384619a0)
- Wirth, C. P., Zhou, G., Quinn, S. N., et al. 2021, *ApJL*, 917, L34, doi: [10.3847/2041-8213/ac13a9](https://doi.org/10.3847/2041-8213/ac13a9)
- Wright, E. L., Eisenhardt, P. R. M., Mainzer, A. K., et al. 2010, *AJ*, 140, 1868, doi: [10.1088/0004-6256/140/6/1868](https://doi.org/10.1088/0004-6256/140/6/1868)
- Wu, Y., & Lithwick, Y. 2011, *ApJ*, 735, 109, doi: [10.1088/0004-637X/735/2/109](https://doi.org/10.1088/0004-637X/735/2/109)
- Zechmeister, M., & Kürster, M. 2009, *A&A*, 496, 577, doi: [10.1051/0004-6361:200811296](https://doi.org/10.1051/0004-6361:200811296)
- Zhou, G., Winn, J. N., Newton, E. R., et al. 2020, *ApJL*, 892, L21, doi: [10.3847/2041-8213/ab7d3c](https://doi.org/10.3847/2041-8213/ab7d3c)
- Zhou, G., Quinn, S. N., Irwin, J., et al. 2021, *AJ*, 161, 2, doi: [10.3847/1538-3881/abba22](https://doi.org/10.3847/1538-3881/abba22)
- Zhou, G., Wirth, C. P., Huang, C. X., et al. 2022, *AJ*, 163, 289, doi: [10.3847/1538-3881/ac69e3](https://doi.org/10.3847/1538-3881/ac69e3)
- Ziegler, C., Tokovinin, A., Briceño, C., et al. 2020, *AJ*, 159, 19, doi: [10.3847/1538-3881/ab55e9](https://doi.org/10.3847/1538-3881/ab55e9)
- Ziegler, C., Tokovinin, A., Latiolais, M., et al. 2021, *AJ*, 162, 192, doi: [10.3847/1538-3881/ac17f6](https://doi.org/10.3847/1538-3881/ac17f6)